https://doi.org/10.5194/egusphere-2026-1824
Preprint. Discussion started: 4 May 2026

High nitrous oxide isotopic variability during denitrification by *Pseudomonas* species bearing NirK and NirS

Noémy Chénier[a,b], Paul M. Magyar[a], Jakob Zopfi[b], Claudia Frey[b], Thomas Kuhn[b], Moritz F. Lehmann[b], Joachim Mohn[a]

[a]Laboratory for Air Pollution / Environmental Technology, Empa, Überlandstrasse 129, Dübendorf, Switzerland
[b]Aquatic and Isotope Biogeochemistry, University of Basel, Bernoullistrasse 30, Basel, Switzerland

Corresponding authors: Joachim Mohn Joachim.mohn@empa.ch & Noémy Chénier Noemy.chenier@empa.ch

Abstract

Nitrous oxide (N_2O) isotopocules provide key insights into microbial nitrogen cycling, but their interpretation requires well-constrained values for both oxygen isotope signatures ($\delta^{18}O$–N_2O) and intramolecular ^{15}N site preference (SP) associated with N_2O production pathways. Site preference is widely used to distinguish N_2O formation pathways because bacterial denitrification is generally assumed to yield SP values near 0 ‰ through canonical NorB-mediated NO reduction. However, the extent to which SP remains stable across physiological states and changing NO reduction pathways remains poorly constrained. Likewise, interpretation of $\delta^{18}O$–N_2O associated with denitrification requires understanding the relative contributions of branching kinetic isotope effects and oxygen atom exchange between nitrite and water during N_2O formation.

Here, we investigated N_2O isotopic signatures during denitrification by *Pseudomonas aureofaciens* (NirK-bearing) and *Pseudomonas chlororaphis* (NirS-bearing) under active-growth and resuspension conditions using quantum cascade laser absorption spectroscopy (QCLAS) and isotope ratio mass spectrometry (IRMS). SP tracked canonical NorB-mediated NO reduction but transiently increased above +10 ‰ during early N_2O production, indicating temporary activity of alternative NO reductases. These dynamics were only resolved through continuous QCLAS measurements, highlighting the importance of time-resolved isotopic observations. While SP remains a useful indicator of NO reduction mechanisms, these results show that even within denitrification, shifts between NO reduction pathways may lead to variable SP signatures.

In parallel, we quantified oxygen atom exchange between nitrite and water using incubations prepared in natural-abundance and ^{18}O-enriched water. Contrary to expectations from denitrifier-method studies, P. aureofaciens exhibited substantial and highly variable oxygen-atom exchange (38–100 %), far exceeding previously reported values (<9 %). In contrast, P. chlororaphis showed consistently high but less variable exchange (~66 %). Resuspension experiments reproduced the characteristic low- and high-exchange behavior reported for these strains under denitrifier-method conditions, demonstrating that these exchange values are specific to the methodological framework and not representative of actively growing systems. These results show that oxygen atom exchange is not governed solely by nitrite reductase identity (NirS vs. NirK) but is strongly modulated by physiological state and metabolic context. As a result, $\delta^{18}O$–N_2O cannot be interpreted as a fixed tracer of denitrification pathways outside the constrained conditions of the denitrifier method.

Together, these findings suggest that denitrifying bacteria may generate N_2O with a broader range of $\delta^{18}O$–N_2O and SP than previously assumed. This calls for a reassessment of N_2O isotopocule interpretations and emphasizes the need to integrate isotopic measurements with physiological and biochemical constraints.

https://doi.org/10.5194/egusphere-2026-1824
Preprint. Discussion started: 4 May 2026

1. Introduction

The intensification of agriculture and fossil fuel combustion over the past century has fundamentally altered the global nitrogen (N) cycle, leading to increased emissions of nitrous oxide (N_2O), a potent greenhouse gas and stratospheric ozone-depleting substance (IPCC, 2023; WMO, 2024). Microbial processes, particularly denitrification – the sequential reduction of nitrate (NO_3^-) to dinitrogen (N_2) via nitrite (NO_2^-), nitric oxide (NO), and N_2O – account for most anthropogenic N_2O emissions (Denman et al., 2007; Reay et al., 2012). However, apportioning N_2O sources among microbial and abiotic pathways remains challenging due to the diversity of processes involved (Yu et al., 2020).

Stable isotope analysis of N_2O provides an important tool to trace microbial processes and identify N_2O sources. Bulk $\delta^{15}N$ and $\delta^{18}O$ values integrate information on substrate origin and isotope fractionation during N_2O formation (Sutka et al., 2006; Toyoda et al., 2005; Denk et al., 2017). In multistep pathways such as denitrification, the apparent isotope effect reflects the combined influence of multiple enzymatic reactions (Ostrom & Ostrom, 2011). The intramolecular site preference (SP), defined as the difference in ^{15}N abundance between the central (α) and terminal (β) positions in N_2O (Yoshida & Toyoda, 1999), is widely used to distinguish microbial formation pathways as it is considered to be largely substrate-independent. Bacterial denitrification typically yields SP values near 0 ‰, whereas fungal denitrification and hydroxylamine oxidation produce higher values (~20–35 ‰) (Toyoda et al., 2005; Frame & Casciotti, 2010; Ostrom et al., 2011; Toyoda et a., 2017; Yu et al., 2020). These low SP values are generally attributed to NO reduction by the canonical nitric oxide reductase NorB. However, recent work has shown that alternative NO detoxification pathways, particularly via flavohemoglobins (Fhp), can produce elevated SP values under high-NO conditions (Wang et al., 2024). These reactions do not represent a separate environmental pathway, but rather an alternative enzymatic fate of NO within denitrifying organisms. Together, these findings demonstrate that while SP remains a powerful discriminator of broad N_2O formation mechanisms, its expression may be more sensitive to which enzymes are involved and to physiological state than is typically assumed.

In contrast, the oxygen isotopic composition of N_2O ($\delta^{18}O$–N_2O) reflects both NO reduction by NorB and upstream processes and depends on the balance between nitrate-derived oxygen, nitrite–water exchange, and branching isotope effects. The extent of oxygen atom exchange between nitrite and water prior to NO reduction is a particular point of variation. Among denitrifiers, two structurally distinct nitrite reductases are found: the cytochrome cd_1-type NirS and the copper-containing NirK. Differences in oxygen isotope exchange between nitrogen oxide intermediates and ambient water have often been attributed to Nir identity, largely based on observations from the bacterial denitrifier method developed for nitrate $^{15}N/^{14}N$ and $^{18}O/^{16}O$ isotope analysis (Casciotti et al., 2002). Under these stationary-phase, washed-cell conditions, *Pseudomonas chlororaphis* subsp. *chlororaphis* (NirS) incorporates a large fraction of oxygen from water into N_2O (39–76 %), whereas the closely related *Pseudomonas chlororaphis* subsp. *aureofaciens* (NirK) shows minimal exchange (~6 %). This contrast has led to the widespread assumption that NirS and NirK impose fundamentally different constraints on $\delta^{18}O$–N_2O expression (Kool et al., 2007).

However, this inference is based on a narrow experimental framework and has not been systematically tested under active growth conditions. Earlier microbiological studies (e.g., Ye et al., 1991) and more recent work in soils and pure cultures report substantial variability in oxygen atom exchange behavior that cannot be

https://doi.org/10.5194/egusphere-2026-1824
Preprint. Discussion started: 4 May 2026

explained by a simple NirK–NirS dichotomy (Lewicka-Szczebak et al., 2016; Rohe et al., 2017; Yu et al., 2020). Whether observed $\delta^{18}O–N_2O$ variability reflects intrinsic enzyme properties or instead arises from physiological state, substrate availability, and reaction dynamics therefore remains unresolved.

The bacterial denitrifier method not only provides well-established information on the behavior of NirS- and NirK-bearing denitrifiers but also serves as a calibration framework for isotopic analyses. Complete conversion of nitrate to N_2O allows direct determination of $\delta^{15}N–NO_3^-$ from $\delta^{15}N–N_2O$ (Sigman et al., 2001). For oxygen isotopes, however only one of the six oxygen atoms originally present in the combined nitrate pool is retained in N_2O, while the others are abstracted and transferred to water during reduction. Under controlled conditions where oxygen atom exchange is low and invariant, the offset between $\delta^{18}O–NO_3^-$ and $\delta^{18}O–N_2O$ remains constant, enabling correction of $\delta^{18}O–N_2O$ measurements (Casciotti et al., 2002). This approach implicitly assumes that oxygen atom exchange remains stable across experimental conditions. If exchange varies with physiological state or reaction dynamics, the $\delta^{18}O–N_2O$ offset is no longer constant, and $\delta^{18}O–N_2O$ cannot be interpreted as a fixed tracer of nitrite reductase identity. Understanding the controls on oxygen atom exchange during denitrification is therefore important both for interpreting $\delta^{18}O–N_2O$ signatures and for evaluating the growth conditions under which the bacterial denitrifier method yields reliable results.

In this study, we investigate how nitrite reductase type, substrate availability, and growth phase influence N_2O isotopic signatures in two closely related denitrifier strains, *P. aureofaciens* and *P. chlororaphis*, both lacking NosZ and therefore accumulating N_2O. We combine (i) real-time measurements of $\delta^{15}N$, $\delta^{18}O$, and SP using quantum cascade laser absorption spectroscopy (QCLAS) with (ii) isotope ratio mass spectrometry (IRMS) analysis of the accumulated product in closed batch incubations to compare active growth and resuspension conditions. This experimental design allows us to separate the effects of physiological state during active growth from those associated with washed-cell resuspension conditions during N_2O production.

Together, this approach addresses a central question: to what extent do N_2O isotopic signatures reflect intrinsic enzyme properties versus differences associated with physiological state and experimental conditions? Resolving this distinction is critical for evaluating the validity and limitations of widely used interpretive frameworks, including the assumed NirK/NirS control on oxygen atom exchange with water and the broader applicability of the bacterial denitrifier method, and the interpretation of SP as a stable proxy for NorB-mediated NO reduction.

2. Material & Methods

2.1 General experimental framework

2.1.1. Bacterial strains

Pseudomonas chlororaphis subsp. *aureofaciens* (formerly *P. aureofaciens*, ATCC 13985) and *Pseudomonas chlororaphis* subsp. *chlororaphis* (formerly *P. chlororaphis*, ATCC 9446) were obtained from the University of Basel Aquatic and Isotope Biogeochemistry culture collection. Growth protocols were adapted from the denitrifier method (Sigman et al., 2001; Casciotti et al., 2002; Weigand et al., 2015).

https://doi.org/10.5194/egusphere-2026-1824
Preprint. Discussion started: 4 May 2026

2.1.2. Overview of the experiments

Two complementary incubation approaches were used to determine how species identity and physiological state influence N_2O isotopic signatures. All experiments were performed in either natural-abundance water (nat) or ^{18}O-enriched water (en), and all media are described in Sect. 2.1.3.

Experiment codes follow the structure X_species_water, where X can be GF for gas flushed incubations or CB denotes closed-batch incubation, CB-R indicates a resuspension assay with nitrate (KNO_3), and CB-RS indicates a resuspension assay using nitrate reference standards. Species can be aur or chlor, which denotes *P. aureofaciens* and *P. chlororaphis*, respectively, and water can be nat and en indicating natural-abundance or ^{18}O-enriched water.

Table 1. Overview of experimental conditions for gas-flushed (GF) and closed-batch (CB) incubations.
Experiments were conducted with *P. aureofaciens* (P. aur) and *P. chlororaphis* (P. chlor) using natural-abundance (nat) or ^{18}O-enriched (en) water. Gas flushed incubations (GF_aur_nat, GF_aur_en, GF_chlor_nat) were performed during active growth under continuous N_2 stripping. Closed-batch incubations include: (i) active-growth experiments in natural-abundance or ^{18}O-enriched water (CB_aur_nat, CB_chlor_nat, CB_aur_en, CB_chlor_en); (ii) stationary-phase resuspension experiments in natural-abundance or ^{18}O-enriched water (CB-R_aur_nat, CB-R_chlor_nat, CB-R_aur_en, CB-R_chlor_en); and (iii) nitrate-standard resuspension assays (CB-RS_aur, CB-RS_chlor) using USGS32, USGS34, IAEA-N3, and ^{18}O-enriched IAEA-N3 (IAEA-N3-spiked).

Experiment ID	Variant	$\delta^{18}O$-H_2O (‰)	Replicates n
Gas flushed incubations (GF)			
GF-aur_nat	P. aur	-9.5	n = 6
GF-aur_en	P. aur	68.3	n = 1
GF3-chlor_nat	P. chlor	-9.5	n = 2
Closed batch incubations (CB)			
CB-aur_en	P. aur	73.5	n = 2
CB-chlor_en	P. chlor	73.5	n = 2
CB-aur_nat	P. aur	-9.5	n = 2
CB-chlor_nat	P. chlor	-9.5	n = 2
CB-R-aur_nat	P. aur	-9.5	n = 2
CB-R-chlor_nat	P. chlor	-9.5	n = 2
CB-RS_aur	P. aur	-9.5 / 780[a]	n = 2
CB-RS_chlor	P. chlor	-9.5 / 780[a]	n = 1

[a]For ^{18}O-enriched resuspension assays with IAEA-N3-spiked, incubation water was prepared by mixing natural water ($\delta^{18}O$ = −9.5 ‰) with ^{18}O-enriched water ($\delta^{18}O$ ≈ +780 ‰), yielding a final $\delta^{18}O$–H_2O of +187.8 ‰ (see Sect. 2.1.4).

Gas-flushed (GF) incubations (GF_aur_nat, GF_aur_en, GF_chlor_nat) were conducted in a temperature-controlled bioreactor under continuous N_2 stripping, allowing real-time quantification of N_2O concentration and isotopic composition during active growth (Fig. 1).

https://doi.org/10.5194/egusphere-2026-1824
Preprint. Discussion started: 4 May 2026

Closed-batch (CB) incubations (CB_aur_nat, CB_chlor_nat, CB_aur_en, CB_chlor_en, CB-R_aur_nat, CB-R_chlor_nat, CB-RS_aur, CB-RS_chlor) were conducted in sealed vials and served three purposes. First, active-growth closed-batch incubations (CB_aur_nat, CB_chlor_nat, CB_aur_en, CB_chlor_en) were conducted in active-growth medium to generate cumulative N_2O for quantifying water–nitrite oxygen exchange during growth. Second, stationary-phase resuspension incubations (CB-R_aur_nat, CB-R_chlor_nat) used pelleted cultures transferred into defined nitrate medium prepared in natural-abundance water. Third, nitrate-standard resuspension assays (CB-RS_aur, CB-RS_chlor) replaced KNO_3 with USGS32, USGS34, IAEA-N3, or ^{18}O-enriched IAEA-N3 (see Sect. 2.1.4).

2.1.3. Culture media

Two distinct media formulations were used depending on experimental objective: an active-growth medium for gas-flushed and closed-batch incubations, and a defined resuspension medium for stationary-phase assays and nitrate-standard experiments. Active growth was carried out in a denitrifier-method medium formulation (Weigand et al., 2015) containing final concentrations of 10 mM KNO_3, 15 mM NH_4^+ supplied as $(NH_4)_2SO_4$, 30 g L^{-1} tryptic soy broth (TSB, Merck Germany), and 5 g L^{-1} K_2HPO_4. Cultures grown in this medium reduced nitrate quantitatively and produced N_2O for isotopic analysis.

For stationary-phase resuspension incubations, actively grown cultures were pelleted and transferred into a simplified medium (Weigand et al., 2015) containing final concentrations of 7.5 mM NH_4^+ supplied as NH_4Cl, 30 g L^{-1} TSB, and 5 g L^{-1} K_2HPO_4. Cell pellets were resuspended in 3 mL of this medium in 20 mL crimp-sealed vials. Vials were purged with N_2 for ~1 h to establish an anoxic headspace and to remove pre-existing gaseous products (including N_2O) prior to initiating the incubation. These conditions were designed to standardize the headspace and remove pre-existing gaseous products prior to incubation, rather than to reproduce the exact conditions of the bacterial denitrifier method. After purging, 20 nmol KNO_3 was added, and cultures were incubated overnight to allow quantitative conversion to N_2O. Thereafter, N_2O was analyzed by GC-IRMS from the vial headspace.

For CB_RS_aur and CB_RS_chlor (closed-batch resuspension assays using nitrate reference standards with *P. aureofaciens* and *P. chlororaphis*, respectively; experiment codes defined in Sect. 2.1.3 and Table 1), the same resuspension procedure was used, except that the 20 nmol KNO_3 addition was replaced by 20 nmol of the respective nitrate isotope standard (USGS32, USGS34, IAEA-N3, or ^{18}O-enriched IAEA-N3-spike.

2.1.4 Characterization of ^{18}O-labelled water

Oxygen exchange between reaction intermediates and water in both GF and CB experiments was assessed using replicate incubations in natural-abundance and ^{18}O-enriched water. The natural water used for all baseline incubations had a $\delta^{18}O$–H_2O = –9.51 ± 0.22 ‰. Two batches of ^{18}O-enriched water were prepared and used: one with $\delta^{18}O$–H_2O = +68.31 ± 0.17 ‰, and a second with $\delta^{18}O$–H_2O = +73.53 ± 0.29 ‰ (Table 1). For nitrate-standard experiments (CB-RS-aur and CB-RS-chlor, Table 1), an ^{18}O-enriched IAEA-N3 spike was prepared by mixing 1 mL of ^{18}O-enriched water ($\delta^{18}O$–H_2O ≈ +780 ‰) with 3 mL of natural water ($\delta^{18}O$–H_2O = −9.5 ‰), yielding a solution with $\delta^{18}O$–H_2O ≈ +187.8 ‰.

https://doi.org/10.5194/egusphere-2026-1824
Preprint. Discussion started: 4 May 2026

The $\delta^{18}O$ isotopic composition of both natural and ^{18}O-enriched waters was measured using a cavity ring-down spectroscopy (CRDS) analyzer (L2130-i, Picarro Inc., USA). Measurements were calibrated on the VSMOW–SLAP scale using three international reference waters: VSMOW2 ($\delta^{18}O$ = 0.00 ± 0.02 ‰), SLAP2 (–55.50 ± 0.02 ‰), and IAEA-607 (+99.02 ± 0.13 ‰), which were measured together with the samples during each analytical run to establish a three-point isotope calibration.

2.1.5 Endpoint N_2O isotopic analysis (IRMS)

Accumulated N_2O produced during incubations was analyzed using gas chromatography coupled to isotope ratio mass spectrometry (GC-IRMS; Delta V Plus coupled to a GasBench system for N_2O purification, Thermo Fisher Scientific, Germany). Isotopic composition was referenced to AIR–N_2 ($\delta^{15}N$) and VSMOW ($\delta^{18}O$) using three laboratory N_2O reference gases (STD1–STD3; ~90 ppm N_2O in N_2) measured alongside samples. Assigned delta values (in ‰) were: STD1: $\delta^{15}N^{\alpha}$ = −22.21 ± 0.39, $\delta^{15}N^{\beta}$ = −49.28 ± 0.40, SP = 27.08 ± 0.56, $\delta^{15}N^{bulk}$ = −35.74 ± 0.07, $\delta^{18}O$ = 26.94 ± 0.23; STD2: $\delta^{15}N^{\alpha}$ = 1.71 ± 0.47, $\delta^{15}N^{\beta}$ = 94.44 ± 0.70, SP = −92.73 ± 0.84, $\delta^{15}N^{bulk}$ = 48.09 ± 0.23, $\delta^{18}O$ = 36.01 ± 0.27; STD3: $\delta^{15}N^{\alpha}$ = 17.11 ± 0.12, $\delta^{15}N^{\beta}$ = −3.43 ± 0.17, SP = 20.54 ± 0.21, $\delta^{15}N^{bulk}$ = 6.85 ± 0.06, $\delta^{18}O$ = 35.39 ± 0.17. Data processing, including scale normalization and correction for ion-source scrambling effects, was performed using the Pylsotopomer package (Kelly et al., 2023).

2.2 Gas-flushed (GF) incubations and online isotope monitoring

2.2.1 Experimental setup for gas-flushed incubations

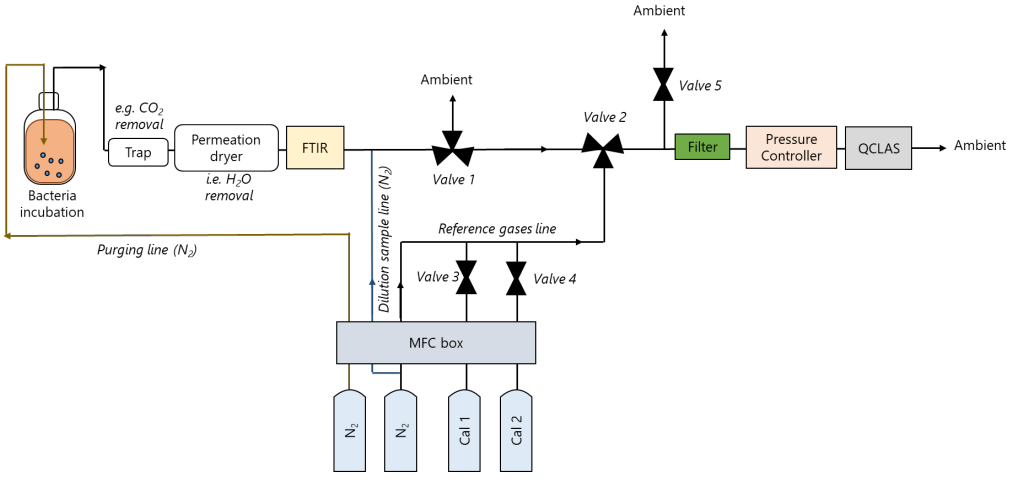

Figure 1. Schematic of the setup applied for bacterial incubations, continuous gas sampling, and real-time analysis of trace gases and N_2O isotopologues. N_2 is used to purge reaction products from the liquid phase via the headspace of the incubation vessel toward the analyzers. Trace gas concentrations (N_2O, NO, residual CO_2 and H_2O) are determined in the CO_2-free and dehumidified sample gas by FTIR spectroscopy. The N_2O concentration is used to set the MFC for N_2 dilution and stabilize the N_2O concentration for QCLAS analysis to xx ppm. Downstream of the FTIR, the gas is directed to the QCLAS for isotopic analysis of N_2O. Calibration of the QCLAS is conducted via automated switching between sample gas and reference standards (valves 1-5). Calibration gas (Cal 1, Cal 2) flows are regulated with mass flow controllers (MFC).

https://doi.org/10.5194/egusphere-2026-1824
Preprint. Discussion started: 4 May 2026

During calibration phases, the sample gas is vented to the atmosphere (valve 1); during measurement phases valves 1, 2 and 5 are switched in parallel, directing the sample gas toward the QCLAS. A pressure controller upstream of the QCLAS stabilizes the multipath cell pressure and ensures stable flow conditions.

For continuous N_2O isotope monitoring under cultivation conditions, strains were grown in the active-growth medium described in Sect. 2.1.2 (Fig 1). Incubations were performed at 30 ± 1 °C for *P. aureofaciens* and 20 ± 1 °C for *P. chlororaphis*, reflecting optimal conditions for growth and N_2O production. Cultures were stirred using a magnetic stirrer to ensure homogeneous mixing, and maintained anaerobic by continuous N_2 flushing (100 mL min^{-1}). Dissolved oxygen, pH (Mettler-Toledo, Switzerland), and optical density (OD_{550}) were monitored throughout the experiments. Substrate consumption was monitored by daily nitrite measurements.. Incubations were typically completed within 5–8 days. Isotopic measurements were stopped, when N_2O concentrations dropped below 50 ppm, whereas concentration measurements by FTIR continued until N_2O levels dropped below detection limits (0.0075 ppm N_2O), confirming complete turnover of nitrogen substrates (Fig. 2). Gas exiting the bioreactor was conditioned prior to analysis; carbon dioxide and water vapor were removed using two consecutive washing bottles containing 1 M NaOH, followed by permeation drying (Perma Pure, USA) (Fig. 1). The CO_2-free, dehumidified sample gas was subsequently filtered through a sintered metal filter (2 µm pore size) and analyzed for trace gas concentrations (N_2O, NO) using an online FTIR analyzer (CX-4000 or CX-4015, Gasmet Technologies, Finland) (Wunderlin et al., 2012). Three-minute average N_2O concentration values were used to calculate dilution ratios and regulate the MFC settings to maintain an approximately constant N_2O concentration (~50 ppm) in the diluted sample gas, which minimized concentration effects on isotope ratio measurements by QCLAS (Wunderlin et al., 2013). Automated sample gas dilution and calibration of the QCLAS system were controlled via a LabVIEW interface (National Instruments Corp., USA) connected to mass flow controllers (Vögtlin Instruments Inc., Switzerland) and electromagnetic valves (Series 9, Parker Hannifin, USA).

2.2.2. Online analysis of N_2O isotopic composition (QCLAS)

Temporally-resolved (1 Hz) N_2O isotopic analysis in the diluted sample gas was performed using a compact quantum cascade laser absorption spectrometer (mini-TILDAS, pathlength 76 m, Aerodyne Research Inc., USA), operated in flow-through mode at a sample pressure of 26.6 hPa (20 Torr) (Ibraim et al., 2018). The instrument simultaneously quantified the concentrations of the four most abundant N_2O isotopologues in the ν_3 absorption band (2203 cm^{-1}): $^{14}N^{14}N^{16}O$, $^{14}N^{15}N^{16}O$ ($^{15}N^{\alpha}$), $^{15}N^{14}N^{16}O$ ($^{15}N^{\beta}$), and $^{14}N^{14}N^{18}O$. Raw concentrations were logged in ASCII format. Time series for each isotopologue were averaged to 60-second intervals as the first step in the data-processing workflow, prior to any correction or calibration. Isotopologue ratios ($^{14}N^{15}N^{16}O/^{14}N^{14}N^{16}O$, $^{15}N^{14}N^{16}O/^{14}N^{14}N^{16}O$, and $^{14}N^{14}N^{18}O/^{14}N^{14}N^{16}O$) were then calculated from these averaged concentrations using a customized R script. Allan deviations at a 60-second averaging time were used to propagate uncertainties in isotope delta values (see Appendix A
).

Two N_2O isotope reference gases diluted in N_2 were used (Mohn et al., 2022); CG1 (RM1A, anchor gas, in ‰): $\delta^{15}N^{\alpha}$ = –0.22 ± 0.46, $\delta^{15}N^{\beta}$ = 0.84 ± 0.46, $\delta^{18}O$ = 39.22 ± 0.15; and CG2 (RM3A, span gas, in ‰): $\delta^{15}N^{\alpha}$ = 50.96 ± 0.47, $\delta^{15}N^{\beta}$ = 53.06 ± 0.47, $\delta^{18}O$ = 103.04 ± 0.16. CG1 was measured every 40 minutes for 10

https://doi.org/10.5194/egusphere-2026-1824
Preprint. Discussion started: 4 May 2026

minutes, to correct for instrumental drift, while the calibration span was determined twice daily analyzing CG1 and CG2. From the measured delta values, the following parameters were calculated: δ^{15}N-bulk = ($\delta^{15}N^{\alpha}$ + $\delta^{15}N^{\beta}$)/2 and SP = $\delta^{15}N^{\alpha} - \delta^{15}N^{\beta}$, following the nomenclature of Toyoda and Yoshida (1999). Data processing steps are detailed in Appendix A.

For validation an independent N_2O isotope reference gas (RM3B) with assigned values of δ^{15}N-bulk = 16.08 ± 0.0 5 ‰, δ^{18}O = 55.17 ± 0.15 ‰, and SP = –0.68 ± 0.91 ‰, was diluted using a two-step diluter (METAS, Switzerland) to a target concentration of 50 ppm N_2O. Measurements were conducted during a short validation campaign in April–May 2024. RM3B was analyzed within the existing CG1/CG2 calibration framework, and the measured values agreed with assigned values within <0.5 ‰ across all isotope parameters.

2.2.3. Isotopic Fractionation Analysis (Rayleigh Model – QCLAS Time Series)

Isotope fractionation during denitrification was assessed using a Rayleigh-type cumulative product model, following the definitions of enrichment factors (ε) provided by Mariotti et al. (1981) and Sutka et al. (2006), which describe the isotopic discrimination between the substrate and the accumulated product over the course of the reaction.

Changes in the isotopic composition of N_2O were modeled as a function of nitrate reduction using the equation:

$$y = a + b \bullet [x] \quad (1)$$

where *y* is the isotopic composition (δ value) of the N_2O product, a and b are fitted coefficients, and [x] represents the reaction progress. The variable [x] was calculated using the Rayleigh equation (Sutka et al., 2006):

$$x = - f \bullet \ln(f) / (1 - f) \quad (2)$$

Here, *f* is the fraction of remaining nitrate, calculated as:

$$f = 1 - (2 \bullet nN_2O / nNO_3^-) \quad (3)$$

where *n* denotes the molar quantities of accumulated N_2O and initial NO_3^-, respectively. The slope *b* corresponds to the apparent enrichment factor ε (in ‰), while the intercept *a* represents the initial isotopic composition of the product pool. This interpretation assumes Rayleigh-type fractionation behavior, i.e. a closed substrate pool with unidirectional consumption and negligible back-reaction. Microbial incubations featuring multistep processes may deviate from these conditions, particularly when O isotope exchange with water or partial recycling of intermediates occurs. Nevertheless, the Rayleigh model provides a useful first-order approximation for comparing fractionation patterns across experiments.

More complex Rayleigh formulations have been proposed to explicitly account for intramolecular isotope effects during N_2O formation, including site-specific treatments of $\delta^{15}N^{\alpha}$ and $\delta^{15}N^{\beta}$ (e.g., Rivett et al., 2025). In the present study, Rayleigh modeling was applied only to δ^{15}N-bulk, for which the standard cumulative product formulation is sufficient.

Fractionation calculations were performed using a custom R pipeline that included uncertainty propagation for N_2O gas concentration, sample gas flow, and the initial substrate amount (NO_3^-). Full computational details are provided in the Appendix A.

https://doi.org/10.5194/egusphere-2026-1824
Preprint. Discussion started: 4 May 2026

2.2.4. Monitoring of nitrate and nitrite during GF incubations and nitrate isotope characterization

During gas-flushed incubations, NO_3^- and NO_2^- concentrations were monitored daily to track substrate depletion and the progression of nitrate reduction. Nitrite was measured spectrophotometrically immediately after sampling using the Griess assay (Hansen and Koroleff, 1999). For nitrate concentration analysis, 1 mL samples were collected daily, filtered through 0.22 µm syringe filters, and stored in Eppendorf tubes at −18 °C prior to analysis. Nitrate concentrations were determined by quantitative reduction to nitric oxide (NO) using acidic vanadium(III), followed by chemiluminescence detection (Braman and Hendrix, 1989).

The isotopic composition of the nitrate substrates used to prepare incubation media was determined prior to the experiments. In addition, selected samples from GF incubations were analyzed to assess changes in the isotopic composition of the residual nitrate pool during denitrification. Nitrate isotope analyses were not performed for closed-batch incubations.

For nitrate isotopic analysis, aliquots containing 20 nmol N were converted to N_2O using the denitrifier method (Sigman et al., 2001; Casciotti et al., 2002). The nitrate stock solution used for all active-growth media had a $\delta^{15}N–NO_3^-$ = +5.7 ± 0.3 ‰ and a $\delta^{18}O–NO_3^-$ = +12.4 ± 0.3 ‰ (n = 3).

Calibration was performed against international nitrate reference materials USGS32 (KNO_3, $\delta^{15}N$ = +180 ‰, $\delta^{18}O$ = +25.4 ± 0.2 ‰), USGS34 (KNO_3, $\delta^{15}N$ = –1.8 ± 0.1 ‰, $\delta^{18}O$ = –27.78 ± 0.37 ‰), and IAEA-N3 (KNO_3, $\delta^{15}N$ = +4.7 ± 0.2 ‰, $\delta^{18}O$ = +25.6 ± 0.4 ‰). Additional reference materials included UBN-1 ($\delta^{15}N$ = +14.15 ‰, $\delta^{18}O$ = +25.7 ‰), Deep Pacific nitrate ($\delta^{15}N$ ≈ +5.0 ‰, $\delta^{18}O$ ≈ +2.0 ‰), and an IAEA-N3-spike standard (IAEA-N3 dissolved in water with $\delta^{18}O–H_2O$ = +780 ‰, see Sect. 2.1.4).

2.3 Closed batch (CB) incubations

2.3.1 Active-growth incubations (natural-water and enriched-water)

Closed-batch incubations were used to generate cumulative N_2O under controlled growth conditions. All experiments were conducted in 500 mL Wheaton bottles containing 400 mL of active-growth medium (Sect. 2.1.2) and incubated at 23 °C for 7 days. Experiments performed in natural-abundance water (CB_aur_nat, CB_chlor_nat) and ^{18}O-enriched-water (CB_aur_en, CB_chlor_en) differed only in the isotopic composition of the water used to prepare the medium. The enriched-water incubations produced $\delta^{18}O–N_2O$ endpoint values that were regressed against $\delta^{18}O–H_2O$ to quantify oxygen atom exchange between nitrite and water. After complete nitrate reduction, accumulated N_2O was analyzed by GC-IRMS (Sect. 2.1.5).

2.3.2 Resuspension incubations in defined nitrate medium (stationary phase)

To obtain stationary-phase $\delta^{18}O–N_2O$ endpoint values, actively grown cultures were pelleted and resuspended in the defined nitrate medium described in Section 2.1.2. These resuspension assays (CB-R_aur_nat, CB-R_chlor_nat) were performed with stationary-phase cultures resuspended in fresh nitrate medium. The experiments were conducted only in natural-abundance water. After overnight nitrate reduction, the accumulated N_2O was analyzed by GC-IRMS (Section Sect. 2.1.5).

https://doi.org/10.5194/egusphere-2026-1824
Preprint. Discussion started: 4 May 2026

2.3.3 Resuspension incubations with nitrate isotope standards (quantification of oxygen isotope exchange)

Additional stationary-phase incubations were performed to quantify oxygen-atom exchange between nitrite and water using nitrate standards with contrasting $\delta^{18}O–NO_3^-$ values (CB-RS_aur, CB-RS_chlor): USGS32, USGS34, IAEA-N3. These were accompanied by an ^{18}O-enriched IAEA-N3-spike to match the typical approach for quantifying oxygen-atom exchange in the bacterial denitrifier method (Sect. 2.1.2). Following quantitative reduction of the added nitrate, $\delta^{18}O–N_2O$ was measured by GC-IRMS (Sect. 2.1.5). The resulting $\delta^{18}O–N_2O$ values were regressed against the known $\delta^{18}O–NO_3^-$ values of the standards. The $\delta^{18}O–N_2O$ versus $\delta^{18}O–NO_3^-$ relationship was applied to derive stationary-phase oxygen-exchange fractions.

This nitrate-standard approach provides an independent estimate of oxygen exchange complementary to the enriched-water experiments (Sect. 2.3.1). Whereas regressions of $\delta^{18}O–N_2O$ versus $\delta^{18}O$ H_2O quantify exchange from the sensitivity of N_2O to water isotopic composition, regressions of $\delta^{18}O–N_2O$ versus $\delta^{18}O–NO_3$ quantify the O-atom exchange from the degree of scale compression relative to nitrate isotope standards. Under conditions of no oxygen exchange, $\delta^{18}O–N_2O$ scales directly with $\delta^{18}O–NO_3^-$ (slope ≈ 1), whereas increasing exchange reduces this dependence (slope < 1). The fraction of oxygen atoms in N_2O derived from water can therefore be estimated from the regression slope (Casciotti et al., 2002).

3. Results and Discussion

3.1 Denitrifying growth and near-quantitative N_2O production in gas-flushed and closed-batch incubations

Both *P. chlororaphis* (NirS-bearing) and *P. aureofaciens* (NirK-bearing) showed consistent denitrifying behavior under anoxic conditions, with N_2O production closely coupled to nitrate reduction. Biomass accumulation and substrate consumption followed the expected progression of anoxic denitrifying growth, indicating that the incubation conditions supported stable and active metabolism throughout.

Biomass increased during the phase of active N_2O production and stabilized as nitrate became limiting, while NO_3^- concentrations decreased in parallel with N_2O formation (Fig. 2C, 2D). This tight coupling indicates efficient conversion of nitrate to N_2O, with only transient accumulation of nitrite (Fig. 2E). This tight coupling indicates efficient conversion of nitrate to N_2O with no substantial accumulation of intermediates. Accordingly, cumulative N_2O yields approached quantitative conversion of the available nitrate (Fig. 2A).

Across gas-flushed incubations, N_2O yields ranged from 60–100 % for *P. aureofaciens* (n = 6) and 50–100 % for *P. chlororaphis* (n = 2), consistent with efficient denitrification under continuous N_2 stripping. Dissolved O_2 concentrations remained below detection (<1 µM), and pH varied only slightly (6.5–7.5), confirming stable anoxic conditions throughout the experiments. Nitrite accumulated transiently during active nitrate reduction but did not persist, indicating rapid turnover within the denitrification pathway.

While such growth dynamics are well established for denitrifying systems (Zumft, 1997), the present gas-flushed setup enables direct observation of N_2O production dynamics under continuous stripping, providing a temporally resolved view that is not accessible in conventional closed systems.

https://doi.org/10.5194/egusphere-2026-1824
Preprint. Discussion started: 4 May 2026

In closed-batch incubations, near-complete nitrate reduction was similarly observed, as indicated by the absence of residual NO_3^- and NO_2^- and the cessation of N_2O production. These results demonstrate that both incubation approaches achieved near-quantitative conversion of nitrate to N_2O under the conditions applied, providing well-constrained systems for isotopic interpretation. N_2O isotopic compositions were determined from endpoint measurements and are discussed in Sect. 3.3 and 3.4.

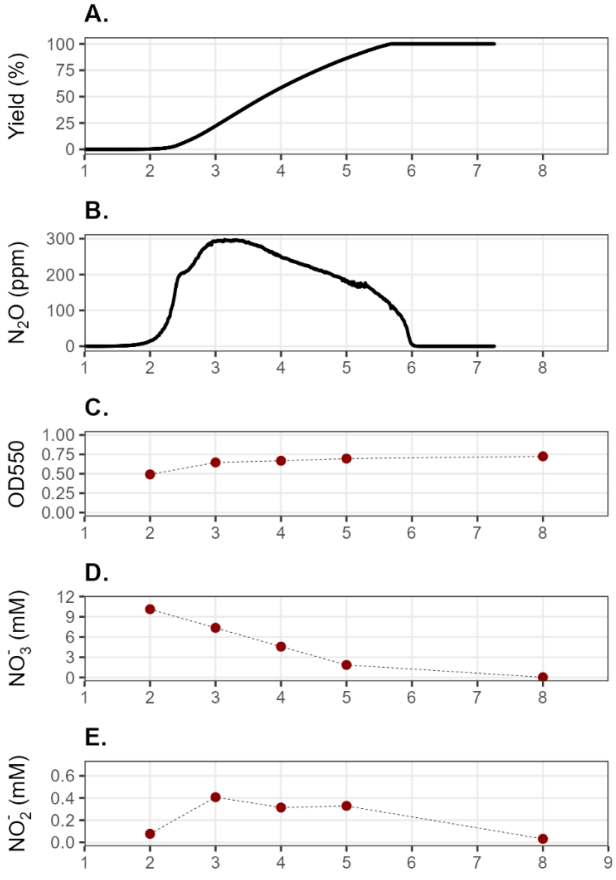

Figure 2. Representative temporal dynamics of N_2O production, cumulative N_2O yield, and culture characteristics during incubation of *P. aureofaciens* (GF_aur). A) Cumulative N_2O yield (% of initial nitrate converted to N_2O); B) Instantaneous N_2O formation, measured in N_2 purge gas; C) Optical density at 550 nm (OD_{550}, circles), as a proxy for biomass accumulation; D) Residual nitrate concentration; E) Nitrite concentration over the course of the experiment.

https://doi.org/10.5194/egusphere-2026-1824
Preprint. Discussion started: 4 May 2026

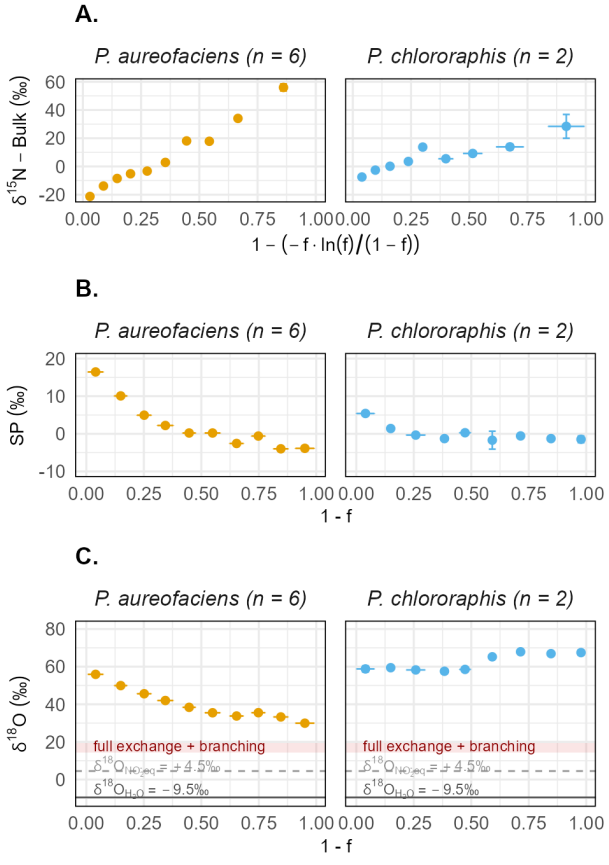

Figure 3. Temporal evolution of N_2O isotopic composition during gas-flushed incubations in natural-abundance water (GF_aur_nat, GF_chlor_nat). Panels show isotopic composition as a function of reaction progress for *P. aureofaciens* (n = 6) (Nirk) and *P. chlororaphis* (n = 2) (NirS). Reaction progress (*f*) was calculated from cumulative N_2O production and re-scaled for each incubation such that the first sampled point corresponds to $f = 0$ and the final point to $f = 1$, allowing comparison across experiments with different final yields. Measurements were grouped into equally spaced bins of reaction progress, and isotopic values were averaged within each bin. Points therefore represent bin-averaged values, with vertical error bars indicating within-bin variability and horizontal error bars indicating the spread in reaction progress of contributing measurements. A) $\delta^{15}N$–Bulk versus the Rayleigh coordinate $1 - \frac{-f \cdot \ln(f)}{1-f}$, which linearizes Rayleigh-type isotope fractionation during substrate consumption. B) Site preference (SP) versus reaction progress ($1 - f$). C) $\delta^{18}O$–N_2O versus reaction progress ($1 - f$). Panels B and C use the simpler ($1 - f$) coordinate to directly visualize temporal trends, whereas panel A uses the Rayleigh transformation to resolve fractionation behavior. In panel C, horizontal lines indicate $\delta^{18}O_{H_2O}$ (−9.5 ‰; solid grey) and $\delta^{18}O_{NO_2,eq}$ (+4.5 ‰; dashed grey). The shaded red band (+14.5 to +19.5 ‰) represents the expected $\delta^{18}O$–N_2O range under full nitrite–water equilibration with branching fractionation.

https://doi.org/10.5194/egusphere-2026-1824
Preprint. Discussion started: 4 May 2026

3.2 Rayleigh-type ^{15}N enrichment in the N_2O pool during nitrate reduction

The $\delta^{15}N$-bulk of accumulated N_2O increased linearly over the course of nitrate reduction in all incubations when expressed against the reaction coordinate $1-(-f \cdot \ln(f)/(1-f))$ (Fig. 3A). This pattern is consistent with Rayleigh-type enrichment expected during unidirectional substrate consumption under closed-system conditions. Enrichment factors ($\varepsilon^{15}N$) were estimated for each incubation by linear regression of $\delta^{15}N$-bulk against the reaction coordinate using the specific reaction progress of each experiment (individual experiment regressions are shown in Appendix B Fig. B1). The rescaling and binning shown in Fig. 3A serve only to visualize common trajectories across incubations.

Enrichment factors ($\varepsilon^{15}N$) derived from this linear Rayleigh approximation ranged from +16 to +55 ‰ (35.5 ± 12 ‰) for *P. aureofaciens* (n = 6) and from +13 to +45 ‰ (25.4 ± 14 ‰) for *P. chlororaphis* (n = 2). Variability across replicate incubations likely reflects differences in nitrate turnover rates and additional biological variability, although no systematic relationship between nitrate reduction rate and $\varepsilon^{15}N$ could be resolved with the present dataset.

The applicability of the linear Rayleigh model is supported by the consistent increase in $\delta^{15}N$-bulk over the reaction coordinate, which reflects the expected kinetic isotope enrichment pattern during progressive substrate consumption (Mariotti et al., 1981). Nevertheless, the linear Rayleigh approximation represents an idealized description when applied to multistep microbial pathways such as denitrification. In such systems, intrinsic isotope effects may be modulated by intermediate pool dynamics, diffusion limitation, or partial reversibility, potentially leading to deviations from a single kinetic fractionation factor. These complexities have been discussed in detail by Haslun et al. (2018) and are not explicitly resolved here. Rather, the Rayleigh analysis is used as a first-order framework to estimate apparent $\varepsilon^{15}N$ values that describe bulk nitrogen isotope enrichment during nitrate reduction and allow comparisons across strains and incubation modes.

To place the $\varepsilon^{15}N$ estimates obtained in this study in context, we compared them with a compilation of fractionation factors for N_2O production from a range of denitrifying organisms and environmental systems (Fig. 4). This dataset, largely derived from Denk et al. (2017), includes values determined under diverse experimental conditions and analytical approaches. The $\varepsilon^{15}N$ values obtained here fall within the broader range reported in the literature and align particularly well with previous results for *Pseudomonas* spp. under nitrate-reducing conditions. Additionally, we include instantaneous isotope effects derived from non-linear Rayleigh formulations, reported as $\eta^{15}N$ values by Haslun et al. (2018). Although expressed using a different notation, these values are conceptually analogous to $\varepsilon^{15}N$ and allow comparison with the fractionation factors derived here. Taken together, these comparisons show that the magnitude of fractionation observed here falls well within the established range for denitrifying systems, indicating that the gas-flushed setup does not introduce atypical isotope effects.

https://doi.org/10.5194/egusphere-2026-1824
Preprint. Discussion started: 4 May 2026

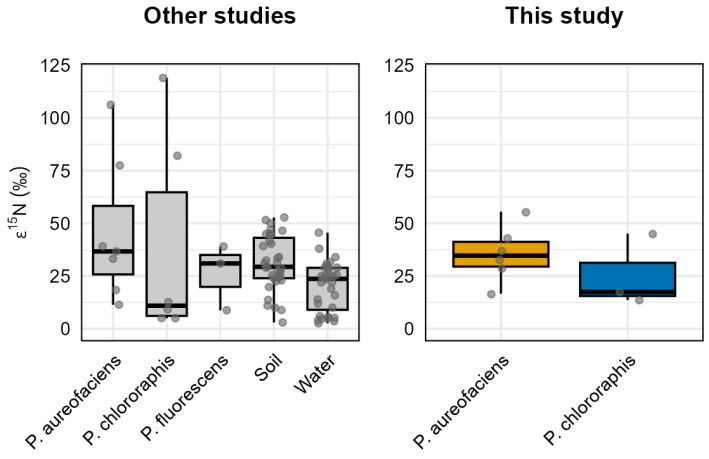

Figure 4. Isotopic enrichment factors ($\varepsilon^{15}N$) for N_2O production across denitrifying microbial communities reported in the literature and observed in this study. Most literature values are compiled from Table S1 of Denk et al. (2017), which integrates isotope effects derived using different experimental systems and modeling approaches (e.g., soils, aqueous environments, pure-culture incubations). Instantaneous isotope effects reported as $\eta^{15}N$ by Haslun et al. (2018) for *P. aureofaciens*, *P. chlororaphis*, and *P. fluorescens* are also included for comparison. For clarity and comparability, all values shown here are expressed using a common sign convention, where positive $\varepsilon^{15}N$ indicates normal isotope effects, i.e., preferential reaction of the light isotope.

3.3 Transient elevated SP suggests variable NO reduction pathways

SP values measured at the endpoint of closed-batch incubations clustered near 0 ‰ for both *P. aureofaciens* and *P. chlororaphis* (Fig. 5B), within the canonical range reported for bacterial denitrification (–8 ‰ to +10 ‰; Yu et al., 2020). This outcome is consistent with the common assumption that SP during bacterial denitrification is invariant and reflects NO reduction by the nitric oxide reductase NorB, which yields values near 0 ‰. This interpretation is supported by measurements from intact denitrifying cultures and by direct assays of purified NorB enzyme (Sutka et al., 2006; Yamazaki et al., 2014; Wang et al., 2024; Rivett et al., 2025; Fig. 5A). Because these measurements integrate N_2O produced over the full course of the reaction, they represent time-averaged isotopic signatures. When assessed using these conventional accumulated-product approaches, N_2O formation appears broadly consistent with NorB-mediated denitrification, although such temporal integration may obscure short-lived deviations from canonical SP behavior.

In contrast to such endpoint observations, our time-resolved dataset shows that elevated SP values (+8 ‰ to +20 ‰) arise transiently but reproducibly during the early stages of N_2O formation under gas-flushed conditions (Fig. 3B; Fig. 5B). Elevated SP values have occasionally been reported in denitrifying cultures. Toyoda et al. (2005), for example, observed SP values up to +22 ‰ in *P. fluorescens*, which they attributed to an abiotic pathway of unknown mechanism. Over the course of nitrate reduction, SP subsequently converged toward ~0 ‰ as the reaction progressed (Fig. 3B). When averaged over the full reaction progress, gas-flushed incubations yielded SP values near 0 ‰, with a slightly elevated median and broader variability compared to

https://doi.org/10.5194/egusphere-2026-1824
Preprint. Discussion started: 4 May 2026

closed-batch endpoint values (Fig. 5B), yet still within the canonical range reported for bacterial denitrification. This convergence toward canonical SP values, despite pronounced early-stage elevations (Fig. 3B), indicates that accumulated N_2O in closed-batch systems integrates over temporally variable production pathways and thereby masks transient deviations in SP. These transient SP elevations are most clearly expressed in *P. aureofaciens* (n = 6). In *P. chlororaphis* (n = 2) they are less apparent in the binned averages due to limited replication and experiment-to-experiment variability, but they are evident in individual incubation trajectories (Appendix B Fig. B1).

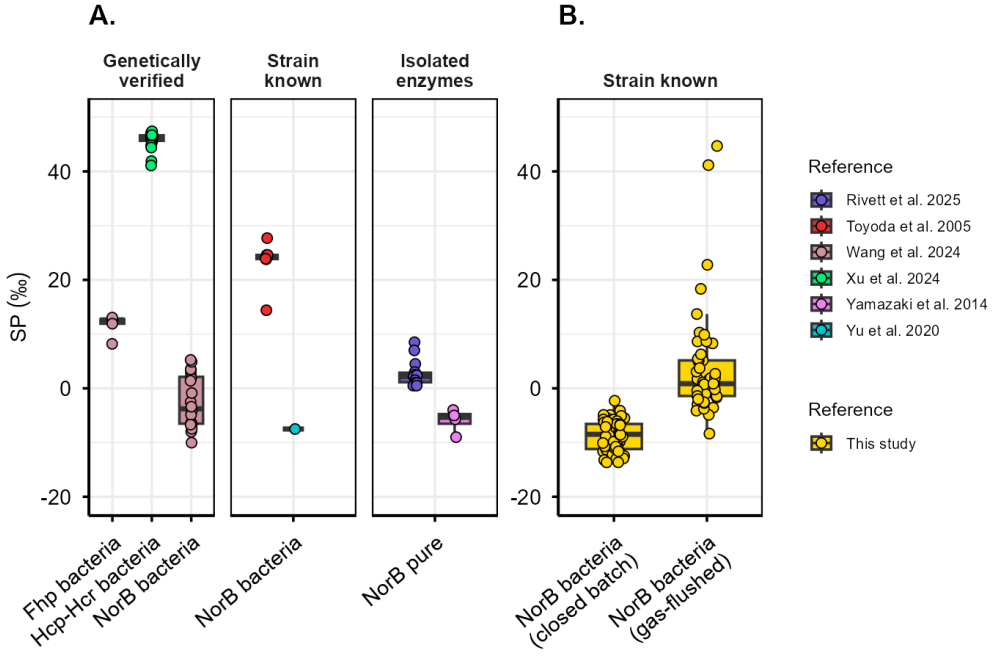

Figure 5. Site preference (SP) of N_2O produced by three classes of N_2O-forming systems. A) Literature-derived SP values grouped by system type: left, intact denitrifiers with genetically verified N_2O-forming enzymes, where both strain identity and the active enzyme system (NorB, Hcp–Hcr, or Fhp) were confirmed (Xu et al., 2024; Wang et al., 2024); center, intact denitrifiers, strains are known but additional N_2O-forming pathways cannot be excluded (Toyoda et al., 2005; Yu et al., 2020); and right, isolated enzyme assays, in which purified NorB was studied directly, yielding enzyme-specific SP values (Yamazaki et al., 2014; Rivett et al., 2025). B) SP values obtained in this study for intact denitrifiers with known strain background, shown separately for closed-batch and gas-flushed incubation modes. Boxplots show the distribution of SP values within each category; horizontal bars indicate mean ± standard deviation. Gas-flushed incubations represent time-resolved SP measurements, whereas closed-batch incubations reflect SP integrated over the accumulated N_2O pool.

Although still within the broader isotopic space reported for bacterial denitrification and related enzyme systems (Fig. 5; Toyoda et al., 2005; Yamazaki et al., 2014; Haslun et al., 2018; Wang et al., 2024; Xu et al., 2024), the consistent early-stage SP elevations suggest that NorB may not be the sole contributor to N_2O formation during the onset of denitrification. One plausible explanation is that rapid NO accumulation during early

https://doi.org/10.5194/egusphere-2026-1824
Preprint. Discussion started: 4 May 2026

Nar/Nir activity initially exceeds the capacity of NorB, such that NO is partially reduced by alternative enzymes until NorB becomes transcriptionally or functionally dominant. Recent work by Wang et al. (2024) directly demonstrated that SP depends on NO reductase identity: NorB activity produced SP values near 0 ‰, whereas flavohemoglobin (Fhp) activity under high-NO conditions yielded elevated SP values of approximately +10 ‰ (Fig. 5A). Using Δ*fhp* mutants and inducible *norB* expression systems, the authors further showed that the balance between these enzymes shifts with growth phase and NO availability. Although the experimental conditions in that study differ from ours, it is plausible that early nitrate respiration in actively growing cultures similarly produces transient NO accumulation combined with low NorB expression, allowing temporary Fhp activity to elevate SP at the onset of denitrification. Future transcriptomic or proteomic analyses would help confirm which NO reductases are expressed during this early phase.

Importantly, several of the transient SP values observed here (Fig. 5B) exceed not only the typical NorB range but also the Fhp-associated values reported by Wang et al. (2024), motivating consideration of additional NO-reducing pathways. Beyond Fhp, other NO detoxification systems may contribute to transient SP variability. Xu et al. (2024) reported N_2O production during dissimilatory nitrate reduction to ammonium (DNRA) and attributed it to the hybrid cluster protein–hybrid cluster reductase (Hcp–Hcr) system based on genomic and transcriptomic evidence (Fig. 5A). While this attribution remains less firmly established than for NorB or Fhp, it defines a distinct high-SP isotopic signature that broadens the reference space for interpreting transient SP behavior. Flavodiiron proteins, which reduce NO to N_2O via asymmetric diiron intermediates (Caranto et al., 2014a, 2014b), are also encoded in many *Pseudomonas* genomes, although their SP signatures remain uncharacterized.

Future work integrating SP-resolved N_2O measurements with transcriptomics, proteomics, or targeted inhibitor assays will be essential to determine which NO reductases are active, when they operate, and how their expression depends on metabolic state and environmental conditions. Taken together, these observations indicate that SP expression during denitrification can be more dynamic than implied by static reference ranges derived from endpoint measurements.

3.4 $\delta^{18}O$ systematics during denitrification across strains and incubation conditions

While site preference primarily reflects the identity of NO reductases operating during N_2O formation, the oxygen isotopic composition of N_2O integrates upstream processes, particularly the extent of oxygen atom exchange between nitrite and water prior to NO reduction. Because nitrite is the immediate precursor to NO, its isotopic composition reflects both oxygen inherited from nitrate reduction and any subsequent equilibration with ambient water. As a result, $\delta^{18}O$–N_2O does not represent a fixed enzymatic property, but rather a composite signal that depends on the relative contributions of nitrate-derived oxygen, nitrite–water exchange, and branching isotope effects. Consequently, its interpretation as a tracer of nitrite reductase identity requires that these processes remain constant – an assumption that has not been tested. Accordingly, $\delta^{18}O$–N_2O patterns are interpreted relative to reference scenarios spanning nitrate-dominated signatures, full nitrite–water equilibration, and intermediate exchange. In the following sections, we examine how $\delta^{18}O$–N_2O varies across strains and incubation conditions as an observational framework, before explicitly quantifying oxygen exchange in Sect. 3.4.2.

https://doi.org/10.5194/egusphere-2026-1824
Preprint. Discussion started: 4 May 2026

3.4.1 Strain-dependent $\delta^{18}O$–N_2O patterns during active growth

A wide range of $\delta^{18}O$–N_2O endpoint values was observed in natural-abundance water incubations under the two active-growth modes (gas-flushed and closed-batch), as summarized in Fig. 6A. In closed-batch incubations, *P. aureofaciens* produced relatively low $\delta^{18}O$–N_2O values (~9 ‰), whereas *P. chlororaphis* yielded substantially higher values (~47 ‰). Under gas-flushed conditions, $\delta^{18}O$–N_2O endpoint values shifted in a strain-specific manner: values for *P. aureofaciens* increased to an intermediate range (26–42 ‰), while *P. chlororaphis* produced consistently elevated values (57–67 ‰). These contrasts indicate a strong incubation-mode sensitivity in *P. aureofaciens*, whereas *P. chlororaphis* exhibits uniformly high $\delta^{18}O$–N_2O expression with comparatively little sensitivity to incubation configuration.

Time-resolved $\delta^{18}O$–N_2O trajectories during gas-flushed incubations further highlights this strain-dependent behavior (Fig. 3C). In *P. aureofaciens*, $\delta^{18}O$–N_2O starts at high values (~50–60 ‰) early in nitrate reduction and declines progressively toward ~30 ‰ as the reaction proceeds. In contrast, *P. chlororaphis* maintains elevated $\delta^{18}O$–N_2O values throughout the reaction, varying within a narrow band around 60 ‰. Thus, under identical conditions, *P. aureofaciens* shows strong variability in $\delta^{18}O$–N_2O, whereas *P. chlororaphis* maintains consistently high values with comparatively little temporal change.

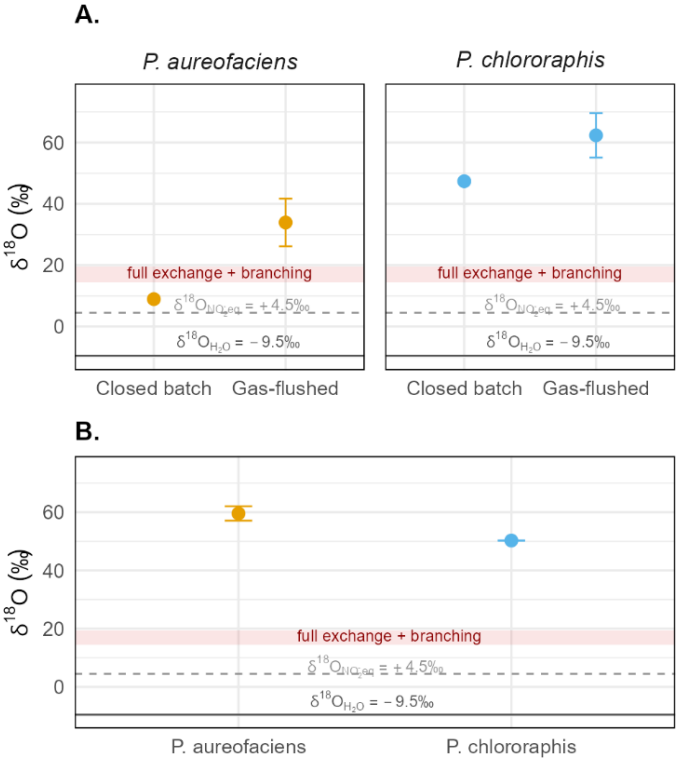

https://doi.org/10.5194/egusphere-2026-1824
Preprint. Discussion started: 4 May 2026

Figure 6. $\delta^{18}O$–N_2O signatures for *Pseudomonas aureofaciens* (NirK) and *P. chlororaphis* (NirS) incubations in natural-abundance water. A) Active-growth incubations. Closed-batch experiments show $\delta^{18}O$–N_2O of the accumulated N_2O pool (n = 2 per strain; mean ± SD). Gas-flushed experiments show final $\delta^{18}O$–N_2O values from time-resolved incubations (*P. aureofaciens*, n = 6; *P. chlororaphis*, n = 2; mean ± SD). B) Resuspension closed-batch incubations following transfer of actively grown cells into fresh nitrate medium (n = 2 per strain; mean ± SD). Horizontal reference lines in both panels indicate $\delta^{18}O_{H_2O}$ (−9.5 ‰; solid grey) and $\delta^{18}O_{NO_2,eq}$ (+4.5 ‰; dashed grey). The shaded red band (+14.5 to +19.5 ‰) represents the expected $\delta^{18}O$–N_2O range under full nitrite–water equilibration with branching fractionation.

To interpret these variable $\delta^{18}O$–N_2O patterns, three reference scenarios can be defined. In the absence of oxygen atom exchange between nitrite and water, $\delta^{18}O$–N_2O is expected to result in values around ~50 ‰, equivalent to the nitrate-source signature ($\delta^{18}O$–NO_3^- = +12.4 ± 0.3 ‰) shifted by the branching isotope effect. If nitrite fully equilibrates with water prior to reduction, its isotopic composition approaches $\delta^{18}O$–NO_2^-,eq = $\delta^{18}O$–H_2O + ε^{18}eq (here +4.5 ‰), resulting in $\delta^{18}O$–N_2O values of +14.5 to +19.5 ‰ after addition of the branching isotope effect (Casciotti et al., 2002, Buchwald & Casciotti, 2010). The $\delta^{18}O$ of water itself (−9.5 ‰) represents a conceptual lower limit approached only by direct incorporation of O atoms from water with no kinetic isotope effects or equilibrium exchange. Because oxygen exchange requires sufficient residence time of nitrite, the transient NO_2^- accumulation observed during active growth (Fig. 2E) provides a mechanistic basis for such exchange.

Against this framework, the two strains exhibit contrasting behavior. *P. aureofaciens*, in closed-batch incubations, yields $\delta^{18}O$–N_2O values below the full exchange plus branching range, indicating extensive oxygen exchange, while gas-flushed conditions produce intermediate values (26–42 ‰), consistent with reduced but still substantial exchange. In contrast, *P. chlororaphis* yields consistently high $\delta^{18}O$–N_2O values under both incubation modes (≈47–67 ‰), clustering near the nitrate-dominated regime and indicating limited equilibration with water.

These patterns are consistent with previous observations under comparable active-growth conditions (Haslun et al., 2018), but here can be interpreted explicitly in terms of oxygen exchange dynamics. Taken together, these results show that $\delta^{18}O$–N_2O reflects the combined influence of nitrate-derived oxygen, oxygen-atom exchange with water, and branching fractionation, which vary with strain and incubation mode. To quantify these contributions, we derived oxygen exchange rates using ^{18}O-enriched water experiments (Sect. 3.4.2).

3.4.2 Quantifying oxygen exchange with water during active growth

To quantify oxygen exchange between nitrite and water during active growth under gas-flushed conditions, *P. aureofaciens* (NirK) was incubated in ^{18}O-enriched water (GF_aur_en; Table 1). $\delta^{18}O$–N_2O values began near ~40 ‰, well below the $\delta^{18}O$ of the enriched water (+68 ‰; Fig. 7). As nitrate reduction progressed, $\delta^{18}O$–N_2O increased steadily, crossed the $\delta^{18}O$-H_2O level, and approached 80 ‰ toward the end of the incubation. Throughout the experiment, $\delta^{18}O$–N_2O remained below values, anticipated for $\delta^{18}O$-NO_2^- under the nitrite–water equilibrium ($\delta^{18}O_{NO_2,eq}$ ≈ +82 ‰) and well below the expected range for $\delta^{18}O$-N_2O derived from fully equilibrated nitrite water combined with branching fractionation ($\delta^{18}O_{NO_2,eq}$ + $\varepsilon^{18}{}_B$ ≈ +91 to +97 ‰; Fig. 7).

This trajectory – beginning below $\delta^{18}O$-H_2O, rising above it, and stabilizing below $\delta^{18}O_{NO_2,eq}$ – indicates that the N_2O product contains a mixture of nitrate-derived and water-exchanged O atoms, with incomplete

https://doi.org/10.5194/egusphere-2026-1824
Preprint. Discussion started: 4 May 2026

approach to full nitrite–water equilibration. The initial $\delta^{18}O$–N_2O values reflect expression of the branching isotope effect under minimal water exchange, whereas the later ^{18}O enrichment reflects the combined influence of branching fractionation and increasing nitrite–water exchange. This behavior is consistent with the elevated $\delta^{18}O$–N_2O endpoints observed for gas-flushed incubations in natural-abundance water (Fig. 3C; Fig. 6A).

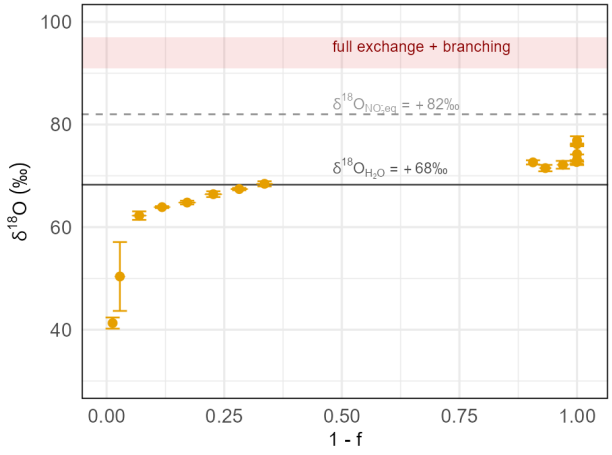

Figure 7. $\delta^{18}O$–N_2O time series as a function of reaction progress ($1 - f$) for incubation of *P. aureofaciens* (NirK) in ^{18}O-enriched water. Horizontal reference lines indicate $\delta^{18}O_{H_2O}$ (+68 ‰; solid grey) and $\delta^{18}O_{NO_2,eq}$ (+82 ‰; dashed grey). The shaded red band (+92 to +97 ‰) represents the expected $\delta^{18}O$–N_2O range under full nitrite–water equilibration with branching fractionation. These references provide a framework to distinguish nitrate-derived oxygen, oxygen-atom exchange between nitrite–water, and branching-related ^{18}O enrichment.

To quantify these processes, $\delta^{18}O$–N_2O values from natural-water and ^{18}O-enriched incubations were combined in $\delta^{18}O$–N_2O vs. $\delta^{18}O$–H_2O regressions (Fig. 8), following the framework of Casciotti et al. (2002). In this approach, the regression slope represents the fraction of oxygen atoms in N_2O derived from water during nitrite reduction, whereas the y-intercept at $\delta^{18}O$–H_2O = 0 ‰ isolates the component of the N_2O oxygen isotope signature independent of water isotopic composition. Under conditions of complete nitrite–water equilibration prior to reduction, the intercept approximates the sum of the nitrite–water equilibrium isotope effect and the branching isotope effect (i.e., $b \approx \varepsilon^{18}_{eq} + \varepsilon^{18}_{B}$; Casciotti et al., 2002, 2007). Deviations from this expectation indicate incomplete equilibration and/or retention of nitrate-derived oxygen in the N_2O product. Closed-batch incubations with *P. chlororaphis* (NirS) exhibited a slope of 0.67 ± 0.05, consistent with partial water exchange (Fig. 8). Its intercept (53.7 ± 4.1 ‰) is strongly elevated relative to ε^{18}_eq + ε^{18}_B (+24 to +30 ‰), reflecting combined contributions from nitrate-derived oxygen, incomplete exchange, and branching effects.

https://doi.org/10.5194/egusphere-2026-1824
Preprint. Discussion started: 4 May 2026

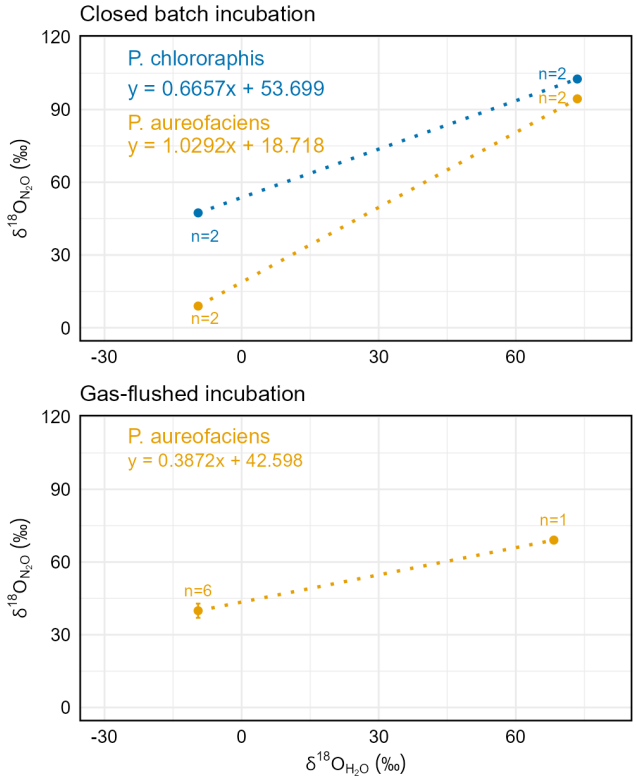

Figure 8. $\delta^{18}O–N_2O$ as a function of $\delta^{18}O–H_2O$ for both endpoint (closed batch) and gas-flushed incubations of *P. aureofaciens* (NirK) and *P. chlororaphis* (NirS). The regression slope from incubations in natural-abundance ($\delta^{18}O–H_2O \approx -9.5$ ‰) and ^{18}O-enriched water ($\delta^{18}O–H_2O \approx +68.3$ ‰ or +73.5 ‰) reflects the extent of oxygen-atom exchange between nitrite and water during stepwise N_2O formation. The intercept represents the $\delta^{18}O–N_2O$ value expected for incubation in water with $\delta^{18}O–H_2O = 0$ ‰, and thus reflects the combined effects of the nitrite–water equilibrium isotope effect and the branching isotope effect for the reaction of $NO_2^- \rightarrow N_2O$, plus any contribution from nitrate-derived oxygen that is not removed by nitite-water exchange. The slope for *P. aureofaciens* in gas-flushed incubation (0.38) indicates partial exchange (38 %), whereas endpoint incubations for *P. aureofaciens* and *P. chlororaphis* suggest near-complete (≈100 %) and partial exchange (≈66 %), respectively.

For *P. aureofaciens*, closed-batch incubations yielded a slope of 1.03 ± 0.06, indicating complete oxygen-atom exchange of nitrite with water during active growth. The corresponding intercept (18.7 ± 4.5 ‰) is at the lower end of values expected for ε^{18}_eq + ε^{18}_B. In contrast, gas-flushed incubation of *P. aureofaciens* yielded a slope of 0.38 ± 0.01, indicating only partial oxygen-atom exchange. The intercept (42.6 ± 1.4 ‰) is substantially higher than both the ε^{18}_eq + ε^{18}_B expectation and the fully exchanged closed-batch intercept, indicating strong retention of nitrate-derived oxygen and enhanced expression of branching fractionation under gas-flushed conditions.

https://doi.org/10.5194/egusphere-2026-1824
Preprint. Discussion started: 4 May 2026

These results demonstrate that oxygen isotope exchange in *P. aureofaciens* during active growth is highly sensitive to incubation conditions, spanning from complete to strongly limited exchange. These contrasts suggest that the canonical low-exchange behavior attributed to NirK is not an intrinsic property of the enzyme, but instead a condition-specific outcome of the denitrifier method.

3.4.3 Stationary-phase resuspension incubations recover canonical Nir-dependent oxygen exchange

To assess whether exchange patterns observed during active growth reflect intrinsic enzyme behavior or experimental conditions, we performed resuspension experiments in which actively grown cultures were pelleted and transferred into a defined nitrate medium. This setup places both strains into a stationary-phase reduction regime closely resembling the bacterial denitrifier method (Casciotti et al., 2002; Weigand et al., 2015).

Resuspension in natural-abundance water produced high and strain-specific $\delta^{18}O–N_2O$ endpoints (Fig. 6B): 59.6 ± 2.5 ‰ for *P. aureofaciens* and 50.3 ± 0.04 ‰ for *P. chlororaphis*. These values lie well above the range expected under full nitrite–water equilibration (~14.5–19.5 ‰), indicating limited oxygen exchange and strong retention of nitrate-derived oxygen, consistent with denitrifier-method observations.

Because endpoint values do not directly constrain exchange, nitrate standards spanning a range of $\delta^{18}O–NO_3^-$ values can be applied to quantify exchange from $\delta^{18}O–N_2O$ vs. $\delta^{18}O–NO_3^-$ regressions. Across both nitrate-standard pairs (USGS32–USGS34 and IAEA-N3–^{18}O-enriched IAEA-N3), the two strains reproduced the canonical low- versus high-exchange behavior reported previously (Casciotti et al., 2002; Appendix B Fig. B2). *P. aureofaciens* exhibited low oxygen exchange (1.5–4.3 %), whereas *P. chlororaphis* showed substantially higher exchange (64.7–76.6 %), in close agreement with published ranges. These results confirm that resuspension experiments recover the expected strain-specific exchange behavior under denitrifier-method conditions.

3.5 Physiological controls on N_2O isotopic signatures: implications for the denitrifier method and interpretation of N_2O isotopocules

The combined isotopic evidence presented here demonstrates that $\delta^{18}O–N_2O$ is strongly controlled by physiological state and experimental conditions, rather than reflecting fixed enzyme-specific properties. Oxygen isotope signatures are modulated by the balance between nitrate-derived oxygen, nitrite–water equilibration, and branching processes, all of which vary with metabolic activity and reaction environment.

A direct comparison across incubation regimes (Fig. 9) reveals a clear contrast. During active growth, oxygen exchange is highly variable: *P. aureofaciens* spans from partial to near-complete exchange (~38 % under gas-flushed conditions to ~100 % in closed-batch incubations), whereas *P. chlororaphis* exhibits consistently higher but more stable exchange (≈66 %). In contrast, under stationary-phase resuspension conditions, both strains reproduce the canonical low- versus high-exchange behavior reported for the denitrifier method, with *P. aureofaciens* showing low exchange (≈2–4 %) and *P. chlororaphis* high exchange (~65–75 %).

This contrast demonstrates that the widely used $\delta^{18}O–N_2O$ signatures associated with NirK and NirS are not intrinsic enzyme properties, but arise under the constrained conditions of the denitrifier method. Outside this

https://doi.org/10.5194/egusphere-2026-1824
Preprint. Discussion started: 4 May 2026

experimental framework, oxygen-atom exchange is dynamic and reflects physiological state rather than nitrite reductase identity alone.

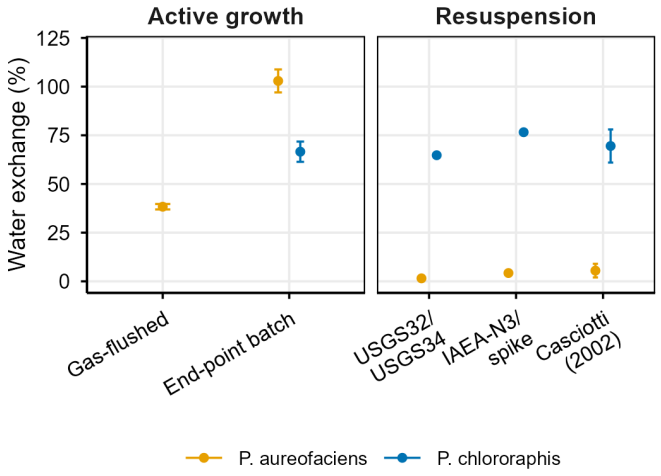

Figure 9. Compilation of water exchange (%) for *P. aureofaciens* (NirK) and *P. chlororaphis* (NirS) under active growth and resuspension conditions. Exchange during active growth was derived from $\delta^{18}O$–N_2O versus $\delta^{18}O$–H_2O relationships using ^{18}O-enriched water (Fig. 8). Under resuspension conditions, exchange was quantified from $\delta^{18}O$–N_2O versus $\delta^{18}O$–NO_3^- regressions using nitrate standards spanning a range of $\delta^{18}O$ values (USGS32/34, IAEA-N3 ± spike), based on the degree of scale compression. These two independent approaches provide consistent constraints on oxygen exchange. For active growth, *P. aureofaciens* showed 38.3 ± 1.4 % (gas-flushed) and 102.9 ± 5.9% (end-point batch) exchange, whereas *P. chlororaphis* showed 66.6 ± 5.2 % (end-point batch). Closed triangles indicate reference values from Casciotti et al. (2002), plotted at the midpoint of reported ranges (2–9 % for *P. aureofaciens*, 61–78 % for *P. chlororaphis*).

A mechanistic explanation for this variability likely lies in the dynamics of the nitrite intermediate pool (Casciotti et al., 2007). Oxygen exchange between nitrite and water requires sufficient residence time of NO_2^- to approach isotopic equilibration. During active growth, differences in nitrate reduction rates, nitrite accumulation, and consumption can alter both the size and lifetime of this intermediate pool, thereby modulating the extent of exchange. Under resuspension conditions, tighter coupling between nitrate and nitrite reduction likely limits nitrite accumulation and constrains exchange. These observations indicate that oxygen exchange reflects system-level metabolic dynamics rather than fixed enzymatic behavior.

Consistent strain-specific differences in $\delta^{18}O$–N_2O under active-growth conditions have been reported previously (Haslun et al., 2018; Sect. 3.4.1). Their agreement with the patterns observed here suggests that such behavior may be more general, but has not been systematically evaluated within a process-based framework.

These findings have important implications for the interpretation of N_2O isotopocules. Application of fixed $\delta^{18}O$–N_2O endmember ranges assumes that oxygen exchange is stable and pathway-specific. The results presented here demonstrate instead that $\delta^{18}O$–N_2O is condition-dependent, and that variability in oxygen isotope signatures reflects changes in exchange dynamics rather than differences in nitrite reductase type. As a

https://doi.org/10.5194/egusphere-2026-1824
Preprint. Discussion started: 4 May 2026

result, $\delta^{18}O–N_2O$ does not provide a reliable tracer of nitrite reductase identity (NirK vs. NirS) outside the constrained conditions of the denitrifier method. Consequently, exchange characteristics derived from denitrifier-method experiments should not be extrapolated to microbial systems without accounting for physiological context. Failure to do so risks systematic misinterpretation of N_2O production pathways. More generally, accurate interpretation of $\delta^{18}O–N_2O$ requires frameworks that explicitly incorporate metabolic state, intermediate dynamics, and environmental conditions, rather than relying on static enzyme-based classifications.

4. Conclusion

The results presented here demonstrate that N_2O isotopic signatures are strongly controlled by physiological state and experimental conditions, rather than reflecting fixed enzyme-specific properties. In particular, $\delta^{18}O–N_2O$ varies extensively with oxygen atom exchange between nitrite and water, which depends on metabolic activity and reaction context. Only under stationary-phase resuspension conditions do enriched-water and nitrate-standard approaches reproduce the characteristic exchange behavior reported in classical denitrifier-method studies. This shows that the widely used $\delta^{18}O–N_2O$ exchange rates are specific to the denitrifier method and do not represent general physiological behavior, but instead reflect the constrained conditions under which the method operates. As a result, $\delta^{18}O–N_2O$ cannot be interpreted as a reliable tracer of nitrite reductase identity outside these conditions.

Site preference (SP) measurements provide complementary, time-resolved insight into N_2O formation pathways during active growth. SP trajectories exhibit a reproducible pattern, with early high values (+10 to +20 ‰) followed by a transition toward values near 0 ‰. These dynamics indicate transient activity of alternative NO reductases, such as flavohemoglobins, during the onset of denitrification, before canonical NorB-mediated NO reduction dominates. Importantly, these shifts occur within the same denitrifying microorganisms and suggest that temporary engagement of NO detoxification pathways may contribute to N_2O formation during phases of elevated NO stress.

These findings have important implications for environmental interpretation of N_2O isotopocules. The application of fixed $\delta^{18}O–N_2O$ or SP endmember ranges assumes that isotopic signatures are stable and pathway-specific constants. Our results demonstrate instead that isotopic expression is conditional. For example, SP values in the range of ~5–15 ‰, often interpreted as evidence for mixed or non-denitrification sources when using fixed endmember frameworks (e.g., Opdyke et al., 2008), can arise entirely from denitrification through shifts in NO reduction pathways. Similarly, variability in $\delta^{18}O–N_2O$ may reflect changes in oxygen exchange dynamics rather than differences in nitrite reductase type, and denitrification may give rise to N_2O with a broader range in $\delta^{18}O–N_2O$ than is typically assumed.

Accurate interpretation of N_2O isotopocules therefore requires frameworks that explicitly account for physiological state, intermediate dynamics, and environmental context, rather than relying on static metabolism or enzyme-based classifications. Constraining process signatures under more realistic environmental conditions (Strubbe et al., 2026) will be essential for improving the interpretation of N_2O isotopic signatures in natural systems. Integrating isotopocule measurements with approaches that resolve metabolic activity and enzyme expression may further help link isotopic signatures to specific microbial processes.

https://doi.org/10.5194/egusphere-2026-1824
Preprint. Discussion started: 4 May 2026

Data availability

The data and code supporting the findings of this study are available from the corresponding author upon reasonable request. The authors intend to deposit the data and analysis code in a public repository prior to final publication.

Competing interests. The authors declare that they have no conflict of interest.

Acknowledgements. This work was supported by the Swiss National Science Foundation (SNSF; grant no. 200020_204907). We thank Tim Paulus for help in learning the methods, Béla Tuzson for support with the laser spectrometer, André Kupferschmid for support with LabView, and Simone Brunamonti for support with the instrument system buildup. We used artificial intelligence tools for code development for data analysis and figure generation, as well as for text editing, paragraph polishing, and grammar correction during the manuscript preparation. All scientific interpretation, analytical decisions, and final manuscript content were reviewed and verified by the authors.

References

1. Braman, R. S. and Hendrix, S. A.: Nanogram nitrite and nitrate determination in environmental and biological materials by vanadium(III) reduction with chemiluminescence detection, *Anal. Chem.*, 61, 2715–2718, doi: 10.1021/ac00199a007, 1989.
2. Buchwald, C. and Casciotti, K. L.: Oxygen isotopic fractionation and exchange during bacterial nitrite oxidation, *Limnol. Oceanogr.*, 55, 1064–1074, doi: 10.4319/lo.2010.55.3.1064, 2010.
3. Caranto, J. D., Weitz, A., Giri, N., Hendrich, M. P., and Kurtz, D. M. Jr.: A Diferrous-Dinitrosyl Intermediate in the N_2O-Generating Pathway of a Deflavinated Flavo-Diiron Protein, *ACS Biochem.*, 53, 5631−5637, doi: 10.1021/bi500836z, 2014a.
4. Caranto, J. D., Weitz A., Hendrich M. P. and Kurtz D. M Jr.: The Nitric Oxide Reductase Mechanism of a Flavo-Diiron Protein: Identification of Active-Site Intermediates and Products, *J. Am. Chem. Soc.*, 136, 7981−7992, doi: dx.doi.org/10.1021/ja5022443, 2014b.
5. Casciotti, K. L., Sigman, D. M., Hastings, M. G., Böhlke, J. K., and Hilkert, A.: Measurement of the oxygen isotopic composition of nitrate in seawater and freshwater using the denitrifier method, *Anal. Chem.*, 74, 4905–4912, doi:10.1021/ac020113w, 2002.
6. Casciotti, K. L., Böhlke, J. K., McIlvin, M., Mroczkowski, S., and Hannon, J.: Oxygen Isotopes in Nitrite: Analysis, Calibration, and Equilibration, *Anal. Chem.*, 79, 2427-2436, doi: 10.1021/ac061598h, 2007.
7. Kenneth L. Denman, Guy Brasseur, Amnat Chidthaisong, Philippe Ciais, Peter M. M Cox, et al.. Couplings between changes in the climate system and biogeochemistry. Solomon, S, D.; Qin, M.; Manning, Z.; Chen, M.; Marquis, K.B.; Averyt, M.; Tignor M.; H.L. Miller. *Climate Change 2007: The Physical Science Basis. Contribution of Working Group I to the Fourth Assessment Report of the Intergovernmental Panel on Climate Change The Physical Science Basis*, Cambridge University Press, pp.499-587, 978-0521-88009-1, 2007.

https://doi.org/10.5194/egusphere-2026-1824
Preprint. Discussion started: 4 May 2026

8. Denk, T. R. A., Mohn, J., Decock, C., Lewicka-Szczebak, D., Harris, E., Butterbach-Bahl, K., Kiese, R., and Well, R.: The nitrogen cycle: A review of isotope effects and isotope modeling approaches, *Soil Biol. Biochem.*, 105 121e137, doi: 10.1016/j.soilbio.2016.11.015, 2016.
9. Frame, C. H. and Casciotti, K. L.: Biogeochemical controls and isotopic signatures of nitrous oxide production by a marine ammonia-oxidizing bacterium, *Biogeosciences*, 7, 2695–2709, doi:10.5194/bg-7-2695-2010, 2010.
10. Granger, J., Sigman, D. M., Lehmann, M. F., and Tortell, P. D.: Nitrogen and oxygen isotope fractionation during dissimilatory nitrate reduction by *Pseudomonas stutzeri*, *Limnol. Oceanogr.*, 53, 2533–2545, doi:10.4319/lo.2008.53.6.2533, 2008.
11. Hansen, H. P., & Koroleff, F. Determination of nutrients. *Methods of Seawater Analysis*, 159-228, doi:10.1002/9783527613984.ch10, 1999.
12. Haslun, J. A., Ostrom N. E., Hegg E. L., Ostrom, P. H.: Estimation of isotope variation of N_2O during denitrification by *Pseudomonas aureofaciens* and *Pseudomonas chlororaphis*: implications for N_2O source apportionment, *Biogeosciences*, 15, 12-3873-3882, doi:10.5194/bg-15-3873-2018, 2018.
13. IPCC: Climate Change 2023: Synthesis Report. Contribution of Working Groups I, II and III to the Sixth Assessment Report of the Intergovernmental Panel on Climate Change, IPCC, Geneva, Switzerland, doi:10.59327/IPCC/AR6-9789291691647, 2023.
14. Kelly C. L., Manning C., Frey C., Kaiser J., Gluschankoff N., Casciotti L. L.: Pyisotopomer: A Python package for obtaining intramolecular isotope ratio differences from mass spectrometric analysis of nitrous oxide isotopocules, *Rapid Commun. Mass Spectrom., 1097-0231,* doi:10.1002/rcm.9513, 2023.
15. Kendall, C., Elliott, E. M., & Wankel, S. D.: Tracing anthropogenic inputs of nitrogen to ecosystems. *Stable Isotopes in Ecology and Environmental Science*, Malden, MA, USA: Blackwell Pub, 238-282, doi: 10.1002/9780470691854, 2007.
16. Kool, D. M., Wrage, N., Oenema, O., Dolfing, J., & Van Groenigen, J. W.. Oxygen exchange between (de) nitrification intermediates and H2O and its implications for source determination of NO and N2O: a review. *Rapid Communications in Mass Spectrometry: An International Journal Devoted to the Rapid Dissemination of Up-to-the-Minute Research in Mass Spectrometry*, *21*(22), 3569-3578, doi: 10.1002/rcm.3249, 2007.
17. Mariotti, A., Leclerc, A., & Germon, J. C.: Nitrogen isotope fractionation associated with the $NO_2^- \rightarrow N_2O$ step of denitrification in soils. *Can. J. Soil Sci.*, 62, 227-241, doi:10.1007/BF02374138, 1981.
18. Mohn, J., Biasi, C., Bodé, S., Boeckx, P., Brewer, P.J., Eggleston, S., Geilmann, H., Guillevic, M., Kaiser, J., Kantnerová, K. and Moossen, H.: Isotopically characterised N_2O reference materials for use as community standards. *Rapid Commun. Mass Specrom., 36,* 13, e9296, doi:10.1002/rcm.9296, 2022.
19. Opdyke, M. R., Ostrom, N. E., & Ostrom, P. H.: Evidence for the predominance of denitrification as a source of N_2O in temperate agricultural soils based on isotopologue measurements. *Global Biogeochemical Cycles*, 23, 4, doi:10.1029/2009GB003523, 2008.
20. Ostrom, N. E., & Ostrom, P. H.: The isotopomers of nitrous oxide: analytical considerations and application to resolution of microbial production pathways, *Handbook of Environmental Isotope Geochemistry,* Vol I pp. 453-476. Berlin, Heidelberg: Springer Berlin Heidelberg, doi:10.1007/978-3-642-10637-8_23, 2011.

https://doi.org/10.5194/egusphere-2026-1824
Preprint. Discussion started: 4 May 2026

21. Reay, D. S., Davidson, E. A., Smith, K. A., Smith, P., Melillo, J. M., Dentener, F., & Crutzen, P. J.: Global agriculture and nitrous oxide emissions, *Nat. Clim. Change,* 2, 410–416, doi:10.1038/nclimate1458, 2012.
22. Rivett, E. D., Finders, C. M., Haslun, J. A., Gandhi, H., Kahle, M., Ädelroth, P., Ostrom, P. H., Ostrom, N. E. and Hegg E. L.: Isotopic Fractionation and Kinetic Isotope Effects of a Purified Bacterial Nitric Oxide Reductase (NOR). *Biochemistry*, *64*, 20, 4327-4340, doi:10.1021/acs.biochem.5c00417, 2025.
23. Rohe, L., Well, R., & Lewicka-Szczebak, D.: Use of oxygen isotopes to differentiate between nitrous oxide produced by fungi or bacteria during denitrification. *Rapid Commun. Mass Spectrom.*, 31, 16, 1297-1312, doi:10.1002/rcm.7909, 2017.
24. Sigman, D. M., Casciotti, K. L., Andreani, M., Barford, C., Galanter, M., and Böhlke, J. K.: A bacterial method for the nitrogen isotopic analysis of nitrate in seawater and freshwater. *Anal. Chem.*, 73, 4145–4153, doi:10.1021/ac010088e, 2001.
25. Strubbe, L., Keck, H., Magyar, P. M., Mohn, J., Joss, A., & Froemelt, A. (2026). Activating specific N2O production pathways to understand emission dynamics in wastewater treatment. *Water Research*, 125580, doi:10.1016/j.watres.2026.125580, 2026.
26. Sutka, R. L., Ostrom, N. E., Ostrom, P. H., Breznak, J. A., Gandhi, H., Pitt, A. J., and Li, F.: Distinguishing nitrous oxide production from nitrification and denitrification using N_2O isotopomers. *Appl. Environ. Microbiol.*, 72, 638–644, doi:10.1128/AEM.72.1.638-644.2006, 2006.
27. Toyoda, S., Mutobe, H., Yamagishi, H., Yoshida, N., and Tanji, Y.: Fractionation of N_2O isotopomers during production by denitrifier bacteria, *Soil Biol. Biochem.*, 37, 1535–1545, doi:10.1016/j.soilbio.2005.01.009, 2005.
28. Toyoda, S., Yoshida, N., & Koba, K. Isotopocule analysis of biologically produced nitrous oxide in various environments. *Mass Spectrometry Reviews*, *36*(2), 135-160, doi:10.1002/mas.21459, 2017.
29. Wang, R. Z., Lonergan, Z. R., Wilbert, S. A., Eiler, J. M., and Newman, D. K. (2024). Widespread detoxifying NO reductases impart a distinct isotopic fingerprint on N_2O under anoxia. *Proc. Natl. Acad. Sci.*, 121, 25 e2319960121, doi: 10.1073/pnas.2319960121, 2024.
30. Weigand, M. A., Foriel, J., Barnett, B., Oleynik, S., and Sigman, D. M.: Updates to instrumentation and protocols for isotopic analysis of nitrate by the denitrifier method. *Rapid Commun. Mass Spectrom.*, 30, 12, 1365-1383, doi:10.1002/rcm.7570, 2025.
31. WMO: Greenhouse Gas Bulletin, World Meteorological Organization, library.wmo.int/idurl/4/69057, 2024.
32. Wunderlin, P., Mohn, J., Joss, A., Emmenegger, L., and Siegrist, H.: Mechanisms of N_2O production in biological wastewater treatment under nitrifying and denitrifying conditions. *Wat. Res.*, *46*, 4, 1027-1037, doi:10.1016/j.watres.2011.11.080, 2012.
33. Wunderlin, P., Lehmann, M. F., Siegrist, H., Tuzson, B., Joss, A., Emmenegger, L., & Mohn, J.: Isotope signatures of N_2O in a mixed microbial population system: constraints on N_2O producing pathways in wastewater treatment. *Environ. Sci Technol.*, 47, 3, 1339-1348, doi:10.1021/es303174x, 2013.
34. Xu, Z., Hattori, S., Masuda, Y., Toyoda, S., Koba, K., Yu, P., & Senoo, K.: Unprecedented N_2O production by nitrate-ammonifying *Geobacteraceae* with distinctive N_2O isotopocule signatures. *mBio*, 15, 12, e02540-24, doi: 10.1128/mbio.02540-24, 2024.

https://doi.org/10.5194/egusphere-2026-1824
Preprint. Discussion started: 4 May 2026

35. Yamazaki, T., Hozuki, T., Arai, K., Toyoda, S., Koba, K., Fujiwara, T., and Yoshida, N.: Isotopomeric characterization of nitrous oxide produced by reaction of enzymes extracted from nitrifying and denitrifying bacteria. *Biogeosciences*, *11*, 10, 2679-2689, doi: 10.5194/bg-11-2679-2014, 2014.
36. Yoshida, N. and Toyoda, S.: Constraining the atmospheric N_2O budget from intramolecular site preference, *Nature*, 405, 6784, 330-334, doi: 10.1038/35012558, 2000.
37. Yu, L., Harris, E., Lewicka-Szczebak, D., Barthel, M., Blomberg, M. R., Harris, S. J., & Mohn, J: What can we learn from N_2O isotopocules? A review of recent progress, *Biogeosciences*, 17, 5513–5537, doi: 10.1002/rcm.8858, 2020.
38. Zumft, W. G.: Cell biology and molecular basis of denitrification, *Microbiol. Mol. Biol. Rev.*, 61, 533–616, 1997.

https://doi.org/10.5194/egusphere-2026-1824
Preprint. Discussion started: 4 May 2026

Appendix A

A1. Calibration of isotopic data provided by Quantum Cascade Laser Absorption Spectroscopy (QCLAS)

Isotopic composition ($\delta^{15}N^{\alpha}$, $\delta^{15}N^{\beta}$, $\delta^{18}O$) of N_2O was derived from uncorrected QCLAS output values (TDL Wintel, Aerodyne Research, USA) using a dedicated R script (IsotopeRead 2.0, N. Chénier, Empa). The processing pipeline includes (i) temporal averaging, (ii) extraction of sample and calibration-gas intervals via external command language (ECL) indices, (iii) drift correction to reference gas CG1, (iv) calibration-factor determination from CG1–CG2 differences, and (v) uncertainty propagation based on Allan deviation and signal intensity.

Data averaging and ratio calculation

QCLAS output data are reported using HITRAN-style shorthand (e.g., 446 equivalent to $^{14}N^{14}N^{16}O$) and averaged over 1-minute time intervals. Isotopologue ratios (e.g. R448) are computed from the concentration of the minor isotopologue (e.g. i448) to the 446 isotopologue:

- R448 = i448/i446
- R456 = i456/i446
- R546 = i546/i446

Temperature stability of the laser and optical cell was verified through automated plotting.

Identification of gas sample and calibration intervals

ECL indices assigned during acquisition were used to identify sample blocks and the two calibration gases (CG1 and CG2). Only intervals with the correct predefined length were retained to ensure consistent calibration.

Calibration gases and normalization

Two N_2O isotope reference gases diluted in N_2 and calibrated to international isotope-ratio scales (Air–N_2 for $^{15}N/^{14}N$, VSMOW for $^{18}O/^{16}O$) by several expert laboratories were used (Mohn et al., 2022):

CG1 (RM1A; anchor gas):

$\delta^{15}N^{\alpha}$ = –0.22 ± 0.46 ‰,

$\delta^{15}N^{\beta}$ = 0.84 ± 0.46 ‰,

$\delta^{18}O$ = 39.22 ± 0.15 ‰

CG2 (RM3A; span gas):

$\delta^{15}N^{\alpha}$ = 50.96 ± 0.47 ‰,

$\delta^{15}N^{\beta}$ = 53.06 ± 0.47 ‰,

$\delta^{18}O$ = 103.04 ± 0.16 ‰

For each sample block, isotopologue ratios were normalized by dividing the sample ratio by the mean CG1 ratio measured immediately before and after the sample:

$$R_X = \frac{R_{X,sample}}{R_{X,CG1}}$$

Calibration-factor determination

https://doi.org/10.5194/egusphere-2026-1824
Preprint. Discussion started: 4 May 2026

Calibration factors (a_x) were calculated from the measured ratio differences between CG1 and CG2 and the known isotopic differences:

$$a_x = \frac{\Delta\delta_X^{(true)}}{\Delta R_{X,meas}}$$

Uncertainty in a_x incorporates both the assigned uncertainty of CG1 and CG2 and the variance of their measured ratios.

Corrected delta values were computed as:

$$\delta X = \left(\frac{R_x}{R x_{CG1}} - 1\right) \times 1000 \times ax + \delta X_{CG1}$$

Uncertainty estimation

Instrumental precision was assessed using the Allan deviation at 60 s spectral averaging and was better than 0.1 ‰ for all δ values.

Uncertainty in $\delta^{15}N^{\alpha}$, $\delta^{15}N^{\beta}$, and $\delta^{18}O$ was assessed by propagating contributions from (i) Allan deviation of the relevant isotopologue ratios, (ii) signal-intensity variability (i446 and minor isotopologues), and (iii) variability in calibration-factors.

The uncertainty for derived quantities was calculated using standard error-propagation rules. For example, site preference (SP = $\delta^{15}N^{\alpha} - \delta^{15}N^{\beta}$) uncertainty was calculated as:

$$\sigma_{SP} = \sqrt{\sigma_{\alpha}^2 + \sigma_{\beta}^2}$$

Uncertainty in $\delta^{15}N$-bulk and $\delta^{18}O$ was propagated analogously from their respective isotopologue components.

Data output

Corrected delta values with propagated uncertainties were exported as .csv files. Diagnostic plots (SP, $\delta^{15}N$-bulk, $\delta^{18}O$) were automatically generated for quality assurance.

All processing was performed in RStudio (RStudio Team, 2020). The full script (IsotopeRead 2.0) is available upon request.

A2. Calculation of N_2O yield and fractionation factors

N_2O yield and isotopic fractionation as well as their uncertainties were calculated using a customized R script (FractionationFactors 1.0, developed by N. Chénier, Empa).

The molar amounts of N_2O (nN_2O) produced during each time interval ΔT were calculated from FTIR-derived concentrations (C_gas in ppm; 10^{-6} L L^{-1}) and nitrogen gas flow rates (Q in mL min^{-1}), using a molar volume of 22.4 L mol^{-1}. NO was treated analogously (n_NO), considering concentrations which exceed the analytical detection limit. For intervals where NO remained below detection, n_NO was not calculated, and no NO yield was reported.

https://doi.org/10.5194/egusphere-2026-1824
Preprint. Discussion started: 4 May 2026

$$nN2O_{gas} = \left(\frac{\left(\frac{Q \times \Delta T}{22.4}\right) \times \left(\frac{C_{gas}}{10^6}\right)}{1000} \right)$$

Uncertainties in N_2O production were calculated by propagation through partial derivatives of the above expression, incorporating both flow and concentration uncertainties. The uncertainty of the measured N_2O and NO concentrations was attributed to either the instrumental detection limit (0.0075 ppm for N_2O and 0.133 ppm for NO), or a relative uncertainty of 10 % for both N_2O and NO, with the larger value used at each time point. Uncertainty in the nitrogen flow rate was assumed to be 0.3 % based on mass flow controller specifications (Vögtlin Instruments Inc., Switzerland).

The N_2O yield (in %) was calculated from the molar amount of N_2O produced over the experiment related to the molar amount of nitrogen substrate (KNO_3, molar mass 101.1 g mol^{-1}). Associated uncertainty was propagated from balance precision (±0.01 g) and purity (≥99 %, conservatively estimated at ±0.5 %).

To calculate Rayleigh-type enrichment factors (ε), the isotopic composition of the accumulated N_2O product gas (δ_{cum}) is required. This was calculated as a weighted average from temporal trends in delta values (δ_i) weighted by the molar amount of N_2O (n_{iN2O}) emitted in the respective time interval. Calculations were performed on synchronized data averaged over 15-minute time intervals:

$$\delta_{cum} = \frac{\sum(\delta_i \times n_{iN2O})}{\sum n_{iN2O}}$$

Uncertainties in δ_{cum} were computed from uncertainties in individual δ-values and the associated molar amount of N_2O. Uncertainties in δ_{cum} were propagated by summing the individual variances associated with δ-values and their corresponding N_2O fluxes. At each time step, the square root of the cumulative variance yielded the standard error used to construct time-resolved confidence intervals for $\delta^{15}N$-bulk, $\delta^{18}O$, and SP.

The fraction of remaining substrate (f) in the Rayleigh reaction progress variable $x = -f \cdot \ln(f)/(1-f)$ was calculated as:

$$f = 1 - \left(\frac{2 \times n_{NO3-}}{n_{N2O}}\right)$$

Uncertainties in f and x were propagated from uncertainties in the molar amount of substrate (n_{NO3-}), calculated from the nitrate mass and its molecular mass, and the cumulative molar amount of N_2O.

Enrichment factors (ε) were obtained by Rayleigh-type regressions, plotting δ values of the accumulated N_2O product gas against the transformed progress variable.

Daily averages, cumulative profiles, and model fits were exported as CSV files. Summary statistics include regression intercept, slope, standard errors, and confidence intervals for each isotopic parameter.

https://doi.org/10.5194/egusphere-2026-1824
Preprint. Discussion started: 4 May 2026

Appendix B

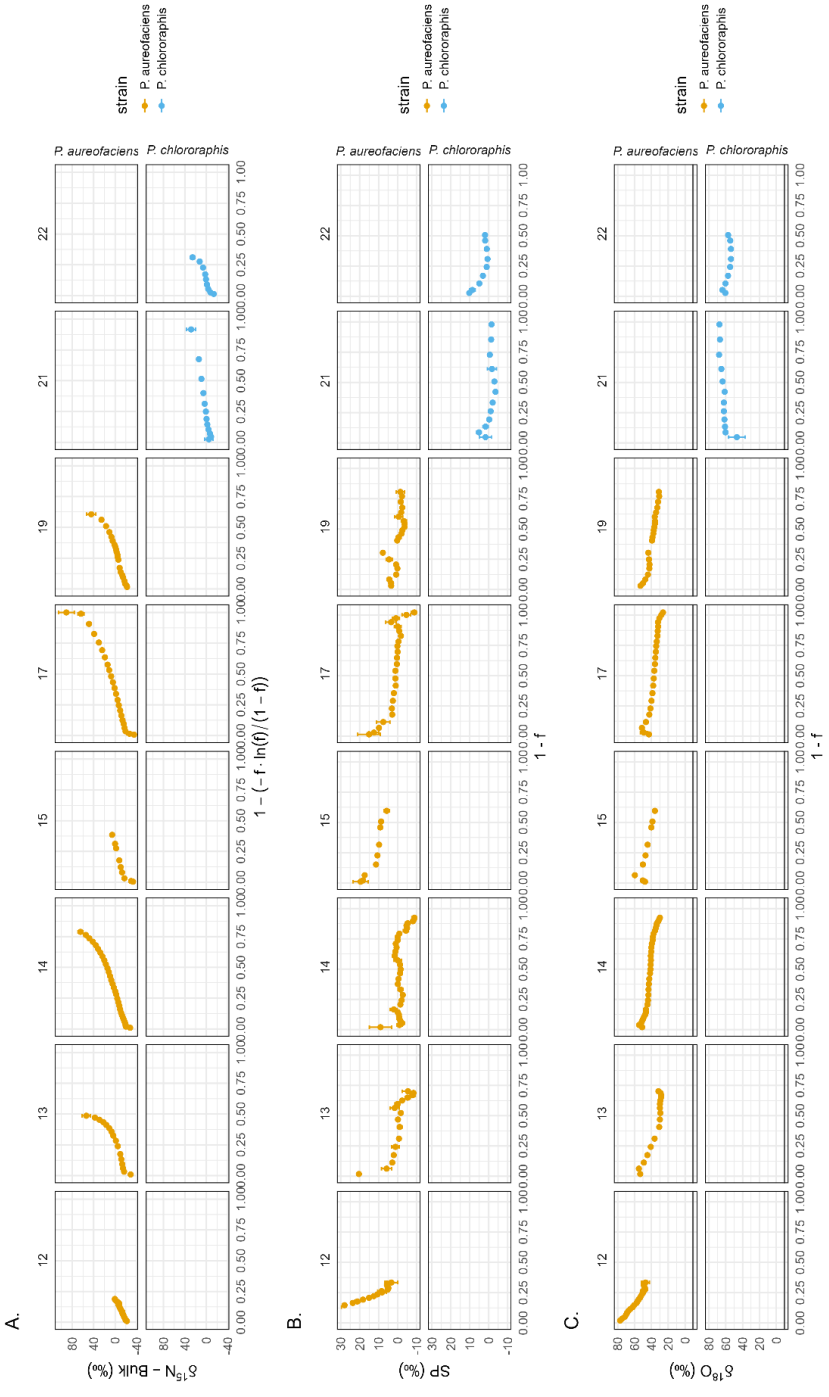

https://doi.org/10.5194/egusphere-2026-1824
Preprint. Discussion started: 4 May 2026

Figure B1. Individual time series for all gas-flushed active-growth incubation experiments shown in Fig. 3. Panels are faceted by strain and by experiment number (numbers at the top of each panel correspond to individual incubation IDs). A. δ^{15}N-bulk, B. site preference (SP), and C. δ^{18}O are plotted as a function of reaction progress, expressed as either $1 - f$ or $1 - (-f \ln f)/(1 - f)$, as indicated on the x-axis. Each point represents an individual measurement; vertical error bars denote analytical uncertainty, and horizontal error bars reflect uncertainty in reaction progress. No binning or normalization across experiments has been applied. In panel C, the short horizontal line in each subplot marks the δ^{18}O of water (−9.5‰). These plots illustrate experiment-to-experiment variability underlying the binned trends presented in the main text.

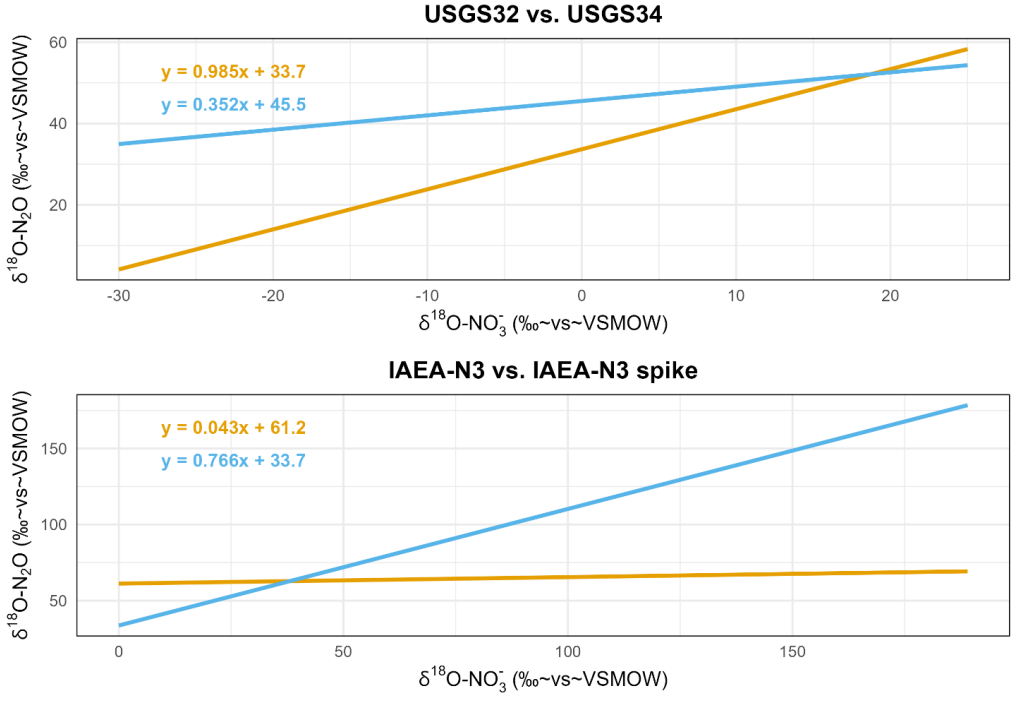

Figure B2. Relationship between δ^{18}O–N_2O and δ^{18}O–NO_3^- in resuspension incubations with international nitrate standards (USGS32/USGS34; IAEA-N3 vs. δ^{18}O-enriched IAEA-N3 spike) for *P. aureofaciens* (orange) and *P. chlororaphis* (blue). Regression slopes quantify the fraction of nitrate-derived oxygen retained in N_2O. For USGS32/USGS34 comparisons, water exchange is calculated as 1 – slope, yielding 1.54 % exchange for *P. aureofaciens* (slope = 0.9846) and 64.8 % for *P. chlororaphis* (slope = 0.3524). For IAEA-N3/spike comparisons, water exchange is estimated directly from the slope, yielding 4.26 % exchange for *P. aureofaciens* (slope = 0.043) and 76.6 % for *P. chlororaphis* (slope = 0.766).